

University of Windsor

Scholarship at UWindor

Electronic Theses and Dissertations

Theses, Dissertations, and Major Papers

2018

Development of a low damping MEMS resonator

Jiewen Liu

University of Windsor

Follow this and additional works at: <https://scholar.uwindsor.ca/etd>

Recommended Citation

Liu, Jiewen, "Development of a low damping MEMS resonator" (2018). *Electronic Theses and Dissertations*. 7377.

<https://scholar.uwindsor.ca/etd/7377>

This online database contains the full-text of PhD dissertations and Masters' theses of University of Windsor students from 1954 forward. These documents are made available for personal study and research purposes only, in accordance with the Canadian Copyright Act and the Creative Commons license—CC BY-NC-ND (Attribution, Non-Commercial, No Derivative Works). Under this license, works must always be attributed to the copyright holder (original author), cannot be used for any commercial purposes, and may not be altered. Any other use would require the permission of the copyright holder. Students may inquire about withdrawing their dissertation and/or thesis from this database. For additional inquiries, please contact the repository administrator via email (scholarship@uwindsor.ca) or by telephone at 519-253-3000ext. 3208.

Development of a low damping MEMS resonator

By

Jiewen (Nicky) Liu

A Thesis
Submitted to the Faculty of Graduate Studies
through the Department of Mechanical, Automotive and Materials Engineering
in Partial Fulfillment of the Requirements for
the Degree of Master of Applied Science
at the University of Windsor

Windsor, Ontario, Canada

2018

© 2018 Jiewen Liu

Development of a low damping MEMS resonator

By
Jiewen Liu

APPROVED BY:

S. Chowdhury

Department of Electrical and Computer Engineering

N. Zamani

Department of Mechanical, Automotive and Materials Engineering

M. Ahamed, Advisor

Department of Mechanical, Automotive and Materials Engineering

Dr. D. Ting, Co-advisor

Department of Mechanical, Automotive and Materials Engineering

January 18, 2018

DECLARATION OF CO-AUTHORSHIP / PREVIOUS PUBLICATION

I. Co-Authorship

I hereby declare that this thesis incorporates material that is result of joint research, as follows:

Chapter 2 of the thesis was co-authored with J. Jaekel, D. Ramdani, and N. Khan under the supervision of Professor M. J. Ahamed. and D. S-K. Ting. In the thesis, the key ideas, simulation running, primary contributions, experimental designs, data analysis, interpretation, and writing were performed by the author. J. Jaekel, D. Ramdani, and N. Khan provided feedback on refinement of ideas and editing of the manuscript.

I am aware of the University of Windsor Senate Policy on Authorship and I certify that I have properly acknowledged the contribution of other researchers to my thesis, and have obtained written permission from each of the co-author(s) to include the above material(s) in my thesis.

I certify that, with the above qualification, this thesis, and the research to which it refers, is the product of my own work.

II. Previous Publication

This thesis includes [*insert number*] original papers that have been previously published/submitted for publication in peer reviewed journals, as follows:

Thesis Chapter	Publication title/full citation	Publication status*
Chapter [2]	<i>J. Liu, J. Jaekel, D. Ramdani, N. Khan, D. S-K. Ting, and M. J. Ahamed, "Effect of geometric and material properties on thermoelastic damping (TED) of 3D hemispherical inertial resonator," ASME 2016, IMECE, Phoenix, USA.</i>	<i>published</i>

I certify that I have obtained a written permission from the copyright owner(s) to include the above published material(s) in my thesis. I certify that the above material describes work completed during my registration as a graduate student at the University of Windsor.

III. General

I declare that, to the best of my knowledge, my thesis does not infringe upon anyone's copyright nor violate any proprietary rights and that any ideas, techniques, quotations, or any other material from the work of other people included in my thesis, published or otherwise, are fully acknowledged in accordance with the standard referencing practices. Furthermore, to the extent that I have included copyrighted material that surpasses the bounds of fair dealing within the meaning of the Canada Copyright Act, I certify that I have obtained a written permission from the copyright owner(s) to include such material(s) in my thesis.

I declare that this is a true copy of my thesis, including any final revisions, as approved by my thesis committee and the Graduate Studies office, and that this thesis has not been submitted for a higher degree to any other University or Institution.

ABSTRACT

MEMS based low damping inertial resonators are the key element in the development of precision vibratory gyroscopes. High quality factor (Q factor) is a crucial parameter for the development of high precision inertial resonators. Q factor indicates how efficient a resonator is at retaining its energy during oscillations. Q factor can be limited by different types of energy losses, such as anchor damping, squeeze-film damping, and thermoelastic damping (TED). Understanding the energy loss-mechanism can show a path for designing high Q resonator. This thesis explores the effects of different design parameters on Q factor of 3D inertial resonators. TED loss mechanisms in a 3D non-inverted wineglass (hemispherical) shell resonator and a disk resonator were investigated. Both the disk and shell share the same vibration modes, and they are widely used as a vibratory resonator shape. Investigation with loss-mechanism shows that robust mechanical materials such as fused silica can offer ultra-low damping during oscillation. TED loss resulting from the effects of geometric parameters (such as thickness, height, and radius), mass imbalance, thickness non-uniformity, and edge defects were investigated. Glassblowing was used to fabricate hemispherical 3D shell resonators and conventional silicon based dry etching was used to fabricate micro disk resonators. The results presented in this thesis can facilitate selecting efficient geometric and material properties for achieving a higher Q-factor in 3D inertial resonators. Enhancing the Q-factor in MEMS based 3D resonators can further enable the development of high precision resonators and gyroscopes.

DEDICATION

To My Parents

ACKNOWLEDGEMENTS

I am thankful to God for giving me the opportunity to pursue my Master program in the University of Windsor. I am grateful to my wonderful parents whose love, encouragement and sacrifice have made me what I am today.

I wish to express my sincere gratitude to my advisor Dr. M. Ahamed for his patient assistance at every step of the way. His guidance has had an immense influence on my professional growth. Without his technical expertise, reviews and criticism, it would not have been possible to shape my paper and this thesis. I would also like to thank my co-advisor Dr. D. Ting for his pushing, positive attitude and professional suggestions. I would like to thank my committee members Dr. N. Zamani and Dr. S. Chowdhury for their valuable suggestions and guidance in the completion of this work.

In the end, I want to thank my fellow graduate students in the Mechanical Engineering Department and the MicroNano Mechatronic Laboratory for their support and encouragement. Studying and working in their friendly company was a memorable experience.

TABLE OF CONTENTS

DECLARATION OF CO-AUTHORSHIP / PREVIOUS PUBLICATION	iii
ABSTRACT	v
DEDICATION	vi
ACKNOWLEDGEMENTS.....	vii
LIST OF TABLES	x
LIST OF FIGURES	xi
NOMENCLATURE	xiii
Chapter 1: Introduction	1
1.1 Background	1
1.2 Literature review	3
1.2.1 Hemispherical Resonator Gyro (HRG)	3
1.2.2 Disc Resonator Gyro (DRG)	7
1.3 Energy loss in MEMS gyro	8
1.3.1 Thermoelastic dissipation	9
1.3.2 Anchor loss	10
1.3.3 Squeeze film damping	10
1.3.4 Surface loss	10
Chapter 2: Thermoelastic energy loss in hemispherical gyro	12
2.1 Introduction.....	12
2.2 Geometric parameters	14
2.3 Mesh Independence	15
2.4 Results and discussion.....	18
2.4.1 Material design	18
2.4.2 Geometric design	20
2.4.3 Geometric non-uniformity.....	24
2.4.3.1 Effect of shell non-uniformity.....	24

2.4.3.2 Effect of gravity center	26
2.4.4 Effect of fabrication inaccuracy	27
2.5 Conclusion	28
Chapter 3: Energy loss in disc resonator gyro	30
3.1 Introduction	30
3.2 Geometric parameters	32
3.2.1 Finite element modeling	32
3.2.2 Mesh independence test	34
3.3 Results and discussion	35
3.3.1 Effect of material properties	36
3.3.2 Effect of disc radius	37
3.3.3 Effect of disc thickness	39
3.3.4 Effect of gap	40
3.3.5 Effect of ellipse disc	42
3.4 Conclusion	43
Chapter 4: Fabrication	45
4.1 Fabrication of hemispherical resonators	45
4.1.1 Introduction	45
4.1.2 Fabrication process	45
4.2 Fabrication of disc resonator gyro [DRG]	47
4.2.1 Introduction	47
4.2.2 Fabrication process	49
4.2.2.1 Spin coating	49
4.2.2.2 Exposure	49
4.2.2.3 Develop	49
4.2.2.4 Dry etching	49
4.2.2.5 Inspection	50
Chapter 5: Conclusion	51
REFERENCES/BIBLIOGRAPHY	54
VITA AUCTORIS	58

LIST OF TABLES

Table 1: Comparison of mode shape among different materials	19
Table 2: Eigenfrequency and Q factor on fused silica and vycor	19
Table 3: Frequency and normalized Q versus Young's modulus respectively when n=4	36
Table 4: Frequency and normalized Q versus density of material respectively when n=4	37
Table 5: Frequency and normalized Q versus <i>Poisson's ratio</i> of material respectively when n=4	37
Table 6: Normalized Q and displacement versus length of long axis of ellipse when n=4	42

LIST OF FIGURES

Figure 1: MEMS gyro developed at Windsor Micro/Nano Mechatronic Lab	3
Figure 2: Hemispherical resonator gyro and its components [18]	6
Figure 3: MEMS disc resonator gyro [22].....	8
Figure 4: Schematic showing different loss mechanisms in inertial resonators.....	9
Figure 5: Schematic of showing geometric parameters and mesh configuration of resonator.....	15
Figure 6. Convergence curve showing optimum mesh configuration	16
Figure 7. Surface map showing n=2 and n=3 mode shapes of the hemispherical resonator.....	17
Figure 8. Cross section surface map at n=2 mode shape	17
Figure 9: Normalized Q and f versus (a) thickness t, (b) height h, and (c) radius r for n=2, respectively	22
Figure 10: Normalized Q versus the ratio of (a) t/h and (b) t/r respectively for n=2.	23
Figure 11 : (a) 3D graph showing Q factor with radius and height of shell	24
Figure 12: Schematic dimensions for non-uniformity in thickness of a resonator....	25
Figure 13: Normalized Q versus the thin edge of the non-uniformity resonator.....	25
Figure 14: Normalized Q factor and frequency versus stem offset from original symmetry point for n=2	27
Figure 15: SEM image shows defects along the edge due to fabrication and the model used in simulating defected surface.....	27
Figure 16: Normalized Q factor (n=2) versus normalized defect parameters simulated with random curved surfaces.	28
Figure 17: Perspective view schematic of an MEMS disk resonator illustrating excitation scheme	30
Figure 18: 3D model about disc resonator with four conformal electrodes in COMSOL	32
Figure 19: (a) Mesh configuration on the disc resonator model.....	34

Figure 20: Convergence curve showing optimum mesh for the disk resonator model.
..... 35

Figure 21: Normalized frequency, Q, and displacement versus disc diameter
respectively when $n=4$ 39

Figure 22: Normalized Q and displacement versus disc thickness respectively when
 $n=4$ 40

Figure 23: Normalized Q and displacement versus disc thickness respectively when
 $n=4$ 41

Figure 24: Frequency versus the value of semi-major axis respectively when $n=4$.. 43

Figure 25: Basic process of glassblowing techniques for hemispherical resonator .. 45

Figure 26: SEM image for fabricated hemispherical resonator 46

Figure 27: Schematic process of fabrication for DRG 48

Figure 28: SEM for fabricated disc resonator device 48

NOMENCLATURE

Generally, symbols have been defined locally. The list of principle symbols is given below.

ρ_0	Initial reference density,	dU	change in internal energy
T_a	absolute temperature	dQ	heat flow into the system
s	entropy per unit mass	dW	work done on the system
σ	Elastic part of the second Piola-Kirchhoff stress	ϵ	Material strain (a tensor).
τ	Inelastic part of the second Piola-Kirchhoff stress	q	heat accumulated per unit volume
w	work done per unit volume	k	thermal conductivity
E	Elastic modulus	ρ_0	Density of material
α	Thermal expansion coefficient	nu	Poisson's ratio
κ	Thermal conductivity	e_p	Relative permittivity
f	Eigenfrequency	τ_t	Thermal relaxation time constant of the system
ω	Resonant frequency	Q_s	Heat source per unit volume
t_b	Beam thickness	l_b	Beam length
c_p	Heat capacity	h	Height of shell
r	Radius of shell	t	Thickness of shell
h_s	Height of stem	r_s	Radius of stem
n	Nodes of mode shape	Q	Quality factor
k_{re}	Effective stiffness	A	Thickness of non-uniformity
τ_t	Thermal relaxation time constant	d	Displacement of nodal point
i_0	Output current	r	Radial displacement of edge
C_0	Static capacitance	V_p	Dc bias voltage

V_i	Amplitude of the ac input signal at the frequency	k	A parameter dependent upon Poisson's ratio
R	Amplitude of displacement on the disc	g_0	Gap between electrodes and disc resonator

Chapter 1: Introduction

1.1 Background

Gyroscopes are physical sensors that can measure the rate of rotation of an object. The development of gyroscopes had a long history. In the mid-19th century, a French physicist, Leon Foucault, named his experimental apparatus for Earth's rotation observation as "gyroscope". His angle measuring mechanical gyroscope was based on a spinning mass [1]. The spinning mass method exploits the exchange of energy between different axes of vibration because of the Coriolis effect [1]. Because of the limitation (such as manufacturing of precision and low friction bearings), the spinning mass is not suitable for long term precision navigation and small scale implementation, even though it was a dominant method of mechanical gyroscope construction in the late 20th century [1]. With the revolution of semiconductor based micro-fabrication technology, Coriolis vibrator gyroscopes development became micro-scale. In a step further, Micro-electromechanical Systems (MEMS) can combine and co-fabricate electrical and mechanical components at microscale inside one single chip. MEMS is a technology used to design and fabricate tiny integrated devices or systems including mechanical and electrical components. MEMS device are fabricated using processes similar to integrated circuit batch processing techniques. These integrated MEMS gyroscope devices are equipped with the ability to sense, control and actuate on the micro scale [2].

MEMS gyroscopes are inertial sensors with micro size. Compared with traditional macro-scale gyroscopes, MEMS gyroscopes offer a wide range of additional advantages, including smaller size, lighter weight, lower cost, and lower excitation power. Hence, MEMS gyroscopes in recent days have seen wide applications in various fields, such as automotive applications for aerospace navigation, electronics for consumers, virtual reality, gaming control, personal navigation, military applications, and so on. For automotive field as an example, automobiles use a yaw rate gyroscope to activate the electronic stability control into the braking system to prevent accidents, or improve stability when they are turning sharply.

Generally, MEMS gyroscopes are equipped with micromechanical sensing part and electronics for actuation and control parts. These are co-fabricated on a single chip or on two separate chips [3][4]. The former one can reduce the size and noise of the device between the mechanical and electronic parts. However, it requires advanced fabrication and package

technology [3]. The latter one has a lower cost, package simplification, and an optimization of mechanical and electronic parts with sensitive outside interference [4].

The development of MEMS gyroscopes has a bit of history. The Draper Laboratory described the first MEMS gyroscope in 1988 [5]. After that, a substantial number of MEMS gyro emerged, such as micro-machined vibrating gyroscopes and piezoelectric vibrating gyroscopes, surface acoustic wave gyroscopes and bulk acoustic wave gyroscopes [6]. These gyroscopes were fabricated using wafer bonding and surface-bulk micro-machining [7].

Micro-machined gyroscopes were categorized into micro-machined vibrating gyroscopes, piezoelectric vibrating gyroscopes, surface acoustic waves, bulk acoustic waves, micro-machined electrostatically suspended gyroscopes and magnetically suspended gyroscope [9]. As shown in Figure 1, a MEMS gyroscope is equipped with small size, low weight, and relatively high precision.

Majority of vibratory MEMS gyroscopes are equipped with a vibrating resonator, which is the sensing element. The resonating mass acts similarly to the spinning wheel in terms of Coriolis Effect. The resonating mass feels a force when a rotation is applied. A vibratory gyroscope with degenerating vibration modes has two resonance modes, including the primary and secondary mode, respectively. The Coriolis force coupling between these two modes help obtain the angular velocity [8]. A proper design is required to effectively couple these two modes and obtain lower frequency split between the two modes.

Effective designing of gyroscope is important prior to fabrication because of higher cost and low turn-around time in fabrication. However, the designing of gyroscopes have various challenges. Compared with pressure and acceleration sensors, MEMS gyroscopes require more factors and variables to be considered. The performance of gyroscopes is sensitive to the potential manufacturing variations, packaging, linear acceleration, temperature, etc. This means that a substantial amount of care (including potential variations) should be taken into consideration, in order to obtain a high performance and low cost of production, during the process of design. Hence, this research was focusing on modeling some key factors of MEMS gyroscopes and finding a way to designing the MEMS gyroscopes with better vibrational performance. To this end, two specific design geometry for the resonating mass were considered; these were hemispherical resonator and disk resonator. Both of these designs are

known to have similar mode shapes with two degenerate modes. Hemispherical resonators are the sensors of choice due to their low damping performance. In the next section, a review on hemispherical and disk resonator is provided.

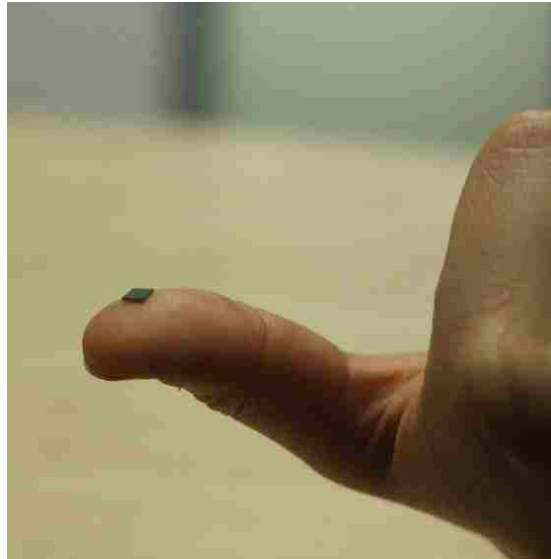


Figure 1: MEMS gyro developed at Windsor Micro/Nano Mechatronic Lab

1.2 Literature review

1.2.1 Hemispherical Resonator Gyro (HRG)

Hemispherical resonator gyroscope (HRG) is well known as ‘wineglass’ gyro. It is a thin hemispherical shell and is usually a wineglass shape. The gyro principle of the HRG rely on the forces arising from Coriolis acceleration. This effect was described by Gaspard-Gustave Coriolis. During the 1900s, an experimental HRG was designed, fabricated and tested, validating the concept of using acoustics for a rotation sensor. The resonator design of the first gyroscope was a wineglass type. The conventional HRG was two inches in diameter and was constructed of aluminum at that time.

In terms of operation, the HRG utilizes the rotation sensitivity of the lowest bending mode of a hemispherical shell, which is called wineglass mode. In a cycle of vibration, this period can be separated into four parts. When the HRG is vibrating in the bending mode, it responds in one cycle of the shell vibration by deforming from spherical to ellipsoidal during the first part of the cycle; then, it returns to be spherical during the second part. Back to back, the HRG deforms into an ellipsoidal shape during the third part, but with the semi-major and semi-minor axes of

the ellipse; after that, it returns to its original spherical shape during the fourth part of the cycle. Hence, the vibrating equatorial ellipse creates a standing wave with four antinodes (locations of maximum displacement) and four nodes (locations of zero displacement). A rotation about the stem of the resonator produces Coriolis forces on the vibrating mass elements when the standing wave is applied in the shell. The overall result is to create the standing wave to change its location on the shell, which can be sensed by the conformal electrodes of the HRG. Figure 2 shows the commercially available wineglass resonator gyroscope with its components.

In a vibrating gyroscope, the resonating mass needs to be oscillating without pumping energy for better sensing performance. The decay in oscillation is due to different energy loss and damping. One parameter quantifying the energy loss is called Quality factor (Q-factor). Inertial sensors with high precision require maximizing its Quality factor (Q-factor) for minimizing energy loss. Q-factor is related to the efficiency of a resonator in retaining energy during oscillations. Q factor can be limited by different types of energy losses, such as anchor damping, squeeze-film damping, and thermoelastic damping (TED). Anchor damping happens when the oscillation of the structure and the anchor, which has a supporting function, creates acoustic waves and results in the loss of energy [2]. In terms of thermo-elastic dissipation (TED), the resonant structure experiences tension and compression when oscillation occurs [3]. Thus, temperature gradients exist and they result in irreversible heat flow, which creates the TED energy loss mechanism [3]. Squeeze film damping often occurs in MEMS device when a released structure is separated from the substrate by a thin layer of gas. When the released structure moves, flow occurs in the thin layer of gas and the resulting energy dissipation produces damping [4].

Q-factor is related to the resonator structure. A resonator with high Q has a good performance in several aspects, such as acceptable precision, good stability, low excitation energy and low energy loss. For the precision of a gyro as an example, a high Q-factor means that the measuring results about a rotational angle taking by this gyro are closer to the real rotational angle. Also, stability of a resonator is relevant to the Q. For example, some gyroscopes can work in the aviation or space exploration, which means that the working temperature is very low. So a high Q can represent that this resonator of the gyro cannot be influenced by the working temperature by a large factor. In terms of excitation energy, a high Q-factor indicates that the gyro excitation requires lower energy. It means that the gyro does not need to pump so much

energy into the resonator in every time when it stops due to its loss mechanism. In terms of energy loss mechanism, a high Q also indicates that a resonator can oscillate longer without more energy excitation.

Recently, 3D micro-scale hemispherical shell resonators have shown the potential to achieve higher Q-factor in the range of 1 million [6], while compatible with MEMS based batch fabrication. In order to get a high Q in MEMS resonator gyro, a significant number of researchers have explored this field to understand the effect of Q factor from geometric and material parameters. For a hemispherical shell resonator, Wang *et al.* reported the experimental demonstration of Q-factor improvement of fused quartz hemispherical resonators after post-fabrication annealing [6]. The effect of thermoelastic dissipation on the Q-factor of shell resonators operating in the wine-glass mode was comprehensively investigated [10]. The ceramic-filled resin-based 3D printed millimeter-wave band-pass filters (BPFs) used a new class of compact high-quality-factor hemispherical cavity resonators [11]. The relationship between the thermoforming parameters of shell during fabrication and the geometric dimension of HRG was discussed in [12].

For a HRG at the macro scale, it was widely used to measure the absolute angle of rotation in the field of inertial navigation. Its Q factor can reach as high as 26 million [13]. Despite these inherent advantages of a macro scale HRG, the fabrication and assembly requirements of this device cost too much, and its relatively large size limits its application. This means that a miniaturization of HRG to micro scale is necessary. However, conventional microfabrication techniques is limited by the thin-film based processes, including photolithography, thin film deposition and wet etching [14]. Recently, Pai *et al.* successfully tested the hemispherical resonator fabricated with planar micro-machining techniques [13]. Rahman *et al.* also developed a new fabrication method for a hemispherical micro glass-shell resonator with glass ball molding as well as a self-guided-alignment process to maintain the gap distance uniform [14].

For a HRG at the microscale, a series of devices about the minimum size made by glass blowing were recently presented. Senkal *et al.* developed and demonstrated a new high temperature micro-glassblowing (in the range of several microns) process for batch fabrication of 3-D low internal loss fused quartz wineglass structures in 2012 [15]. In 2013, they presented a micro-glassblowing resonator showing a Q-factor of 40,000 at 14.8 kHz with 4.2 mm diameter,

50 μm thickness and 300 μm stem [16]. In the following years, Rahman *et al.* fabricated a micro glass-shell resonator with 1 mm diameter and 1.2 μm thickness. It produced resonance at 5.843 kHz with a quality factor of 730 [17].

Technically, an ultra-low damping can be reached only if all the energy dissipation mentioned above is minimized in the design stage. In the second chapter of this thesis, the investigation focuses on how to minimize the thermoelastic energy dissipation to obtain a high Q-factor. In order to improve the precision of the analytical prediction of TED, numerical methods, including finite element analysis, can be utilized to investigate the energy propagation on the substrate of resonators, which will be discussed later in Chapter 2.



Figure 2: Hemispherical resonator gyro and its components [18]

This thesis investigates the effects of shell thickness non-uniformity, edge defects, shell material, gravity center offset and surface defects. TED loss mechanisms in 3D, non-inverted, and wineglass hemispherical shell resonator.

1.2.2 Disc Resonator Gyro (DRG)

Besides the above hemispherical shapes of resonators, disc resonator gyroscopes (DRG) are also popular and widely used in the commercial gyro design. Similar to HRGs, DRGs are also vibrating gyro and shares the similar degenerate mode shape of HRG. However, DRGs can be easily fabricated using different conventional micro-fabrication techniques. Disc resonator gyroscopes incorporating compact optimized electronics are used in inertial reference units and inertial measurement units [6]. They have advantages such as smaller size and weight, less power, and less cost, due to the general mass production implications of MEMS devices. Figure 3 shows a MEMS disc resonator gyroscope.

Significant investigations have been done from design and fabrication aspects of DRGs. Wang et al. demonstrated that the first CVD (Chemical vapor deposition) micromechanical disk resonator made of nanocrystalline diamond with material-mismatched stem recorded a frequency of 1.5 GHz with a Q of 1155 [5]. They also investigated a new fabrication methodology that allows self-alignment of a micromechanical structure to its anchor. For the polysilicon disk resonators, this methodology has been used to achieve Q higher than 2650 on vibrating radial-contour mode with resonance frequency up to 1.156 GHz in both vacuum and air [10]. Oscillators also benefit substantially from high Q, because their phase noise at important offsets was often inversely proportional to the square of Q [10]. Self-alignment of a micromechanical structure was verified to get a high Q. This technique allows its anchor to achieve vibrating radial-contour mode micromechanical disk resonators with record resonance frequencies up to 1.14 GHz and measured the Q at this frequency higher than 1,500 in both vacuum and air [19][19]. A vibrating radial contour mode mechanical disk resonator was presented with a measured frequency and Q of 156 MHz and 9,400, respectively by Clark *et al.* [20]. Even for a disc resonator without a stem, [21] demonstrated that the wineglass mode polysilicon micromechanical disk resonators had achieved a Q of 7.2×10^{12} (the highest at that time), by getting rid of the anchor-to-disk misalignment error, as well as minimizing the perimeter nodal supports.

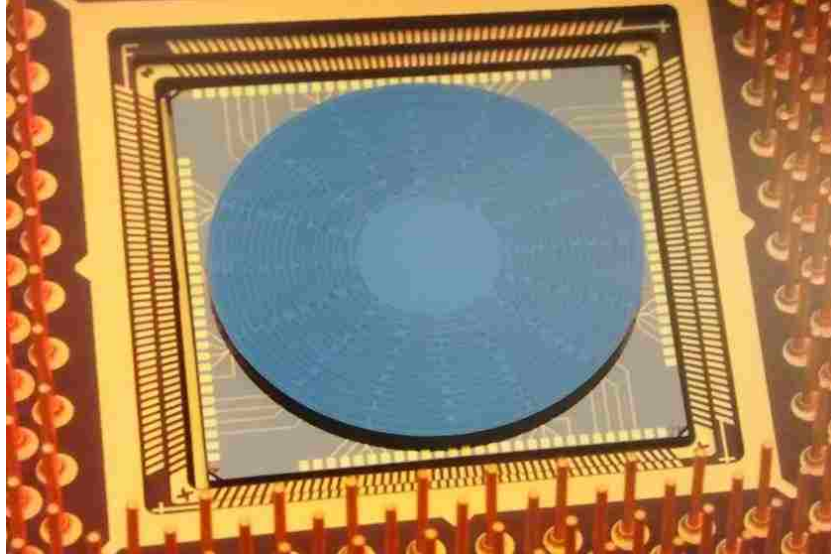


Figure 3: MEMS disc resonator gyro [22]

However, the change of Q factor with other manufacturing and geometric factors (such as manufacturing in accuracy) were not investigated. Based on the previous research, I considered a 3D disc structure resonator and investigated its Q-factor changes with respect to different geometric and fabrication parameters, including disc diameter, non-uniformity effect, gap between the disc and electrodes, and disc material properties.

1.3 Energy loss in MEMS gyro

In order to design high precision MEMS gyroscopes, the loss mechanism and energy dissipation of inertial sensors needs to be modeled for optimum design. Many researchers contributed to this factor in the recent decades. Since 1950s, the mechanical dissipation on resonators was a serious challenge for scientists and engineers. Since that time, a substantial number of previous research for advanced fabrication techniques and the study of loss dissipation mechanism has emerged and been improved. In 2000, Yasumura *et al.* completed a study about the size effects on MEMS structures [23]. These insights and modeling tools have enabled MEMS resonators with high performance matching or exceeding that of macro-scale devices [5]. The energy dissipation mechanism can be classified into four main types, including thermoelastic dissipation (TED), anchor loss, squeeze film damping, surface loss and many other kinds of small damping as shown in Figure 4.

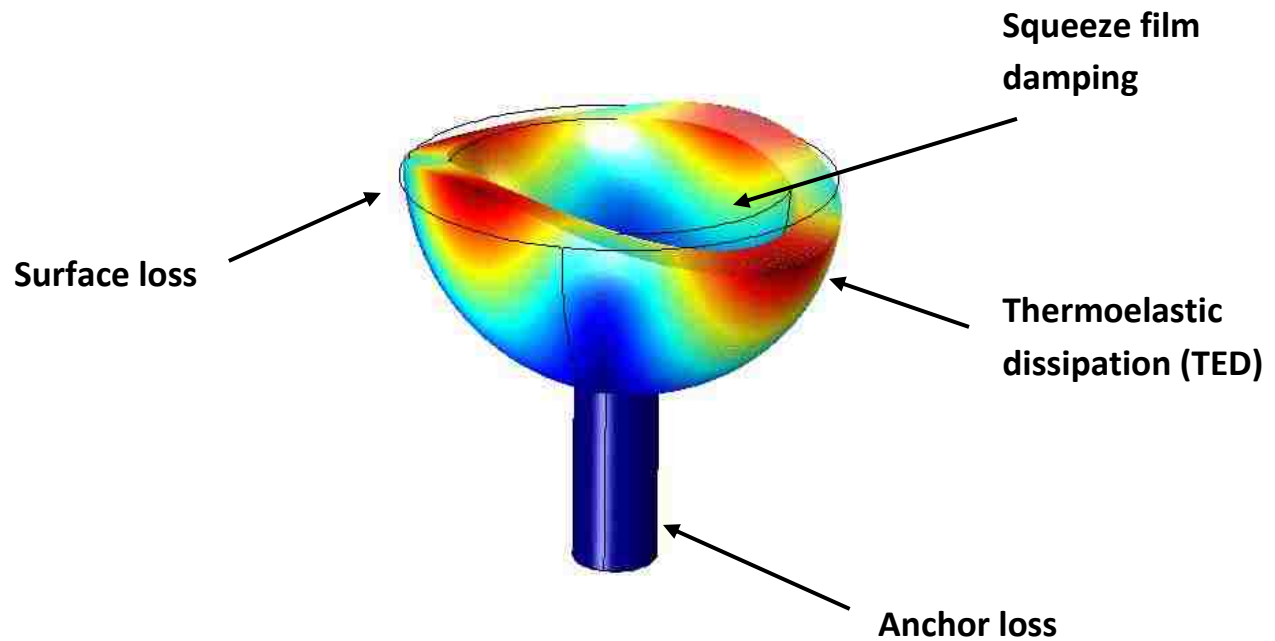


Figure 4: Schematic showing different loss mechanisms in inertial resonators

1.3.1 Thermoelastic dissipation

To analyze the thermoelastic dissipation, here it can be assumed that the resonant structure is under oscillation, which means that this elastic structure can stretch or compress. When such a resonant device is stretched uniformly and reversibly, its temperature drops gradually [24]. The decreased temperature compensates for the increase in entropy. The entropy is caused by the stress in the structure. This is mainly because the process is reversible (the entropy remains constant). The compression of the structure, similarly, experiences an increase in temperature. When such a resonant structure vibrates in a more complex mode shape, there are some regions of compression and some of extension. Depending on the timescale of the vibration, an amount of heat will be transferred from the warmer parts of the structure to the cooler parts [24][25]. As the heat flow is an irreversible process, it is associated with energy loss from the vibrational mode, causing damping for the resonant mode of structure [24][25]. Thermoelastic dissipation is particularly important in MEMS resonators, and it accounts for a high portion of the energy loss mechanism.

1.3.2 Anchor loss

Anchor loss is another type of the energy loss mechanism. Anchor loss happens when the vibration of the resonant structure and its supporting anchors excites acoustic waves that are propagating in the substrate [26]. These acoustic waves are radiated away from the resonator, and they lead to a loss of mechanical energy [26]. In many other cases, anchor loss can represent the main loss mechanism that determines the resonator quality factor. Modifications in the anchor design can drastically affect the coupling of the resonant mode shape to the substrate. For the following chapter in this thesis, the bonding point of anchor and shell of HRG can vary the quality factor of the device. Anchor loss also takes a certain portion of energy loss mechanism in resonant structures.

1.3.3 Squeeze film damping

A resonator gyroscope is usually in close proximity to a stationary surface that acts as electrodes. The gap between the two surfaces forms the parallel plate electrodes. This means that the damping results from the squeezing of a thin film of gas between the two surfaces [26]. The squeezing action pushes the gas between the two plates, which results in a damping force that prevents mechanical contact between the two surfaces [27]. The opposite effect takes place when the surfaces move away from each other because gas is drawn back into the bearing. Squeeze film damping cannot be neglected, even though it is a small amount of energy loss mechanism in resonant structures.

1.3.4 Surface loss

Surface loss is the mechanical energy loss that is caused by surface defects, including dangling bonds, adsorbates (dust), and crystal termination defects. Surface loss matters when the dimensions of MEMS resonators are decreased and the surface-to-volume ratio increases. Until now, many research groups identified an important scaling trend in the measured dissipation, which investigates the Q decreases as surface-to-volume ratios increase [28]. Hence, Weinberg *et al.* offers the hypothesis that a dominant mechanism is the loss due to coupling to

electronic defects on the silicon surface [28]. In my thesis, Chapter 2 investigates and simulates how the edge defects affect the Q during the vibration of a resonator.

1.4 Motivation

In order to design a MEMS gyroscope with high sensitivity and low energy consumption, the inertial resonators are required to have a high Q factor. Energy loss of different forms reduces the Q factor of a resonator. Despite the significant fabrication success, understanding the loss-mechanism in the inertial sensors remains critical in order to show a clear path for successful development of an ideal MEMS resonator with high Q (in the range of several millions). My thesis studied the Q factor of hemispherical shell and disc resonators, respectively. The relationships among Q factor, geometric dimensions (such as thickness and radius) and material properties of a resonator (such as Young's modulus and density) are numerically investigated in the following chapters. Next, the fabrication process of a hemispherical shell resonator and disc resonator, including details, are listed and analyzed.

Chapter 2: Thermoelastic energy loss in hemispherical gyro

2.1 Introduction

Finite element modeling technique using commercially available COMSOL Multiphysics is used to solve TED loss mechanisms in a 3D hemispherical resonator. 3D-dimension space was applied to create the hemispherical wineglass (mode shape) resonator as a 3D model. Thermoelasticity and eigenfrequency were solved together to estimate the thermoelastic damping loss and to solve the Q-factor.

Resonance frequency and Q factor are the important parameters of a resonator. In gyroscope applications, a MEMS resonator is driven at its resonant frequency by a feedback loop to produce a circuit that oscillates at a fixed frequency. For the applications of MEMS resonators, a quality factor of a resonator and the stability of its resonant frequency determine its ultimate performance. Higher-Q resonators have a sharper peak in their frequency spectrum at the resonant frequency. For some resonant modes, the limitation to achieve high Q factor is determined by a thermoelastic damping loss mechanism.

The following analysis makes the computing of the resonance frequency and Q factor of an inertial resonator. Here it is assumed that thermoelastic damping is the dominant damping mechanism. The coupled equations of thermoelasticity will be solved within the resonator in COMSOL Multiphysics.

Thermoelelastic damping in the inertial resonator is based on the first law of thermodynamics, which can be illustrated as follows [29][30][31]:

$$dU = dQ + dW \quad (1)$$

(where dU is the change in internal energy, dQ is the heat flow into the system and dW is the work done on the system.)

For a small part of a solid with an initial reference density ρ_0 , the first law can be changed to the following equation:

$$du = T_\alpha ds + \frac{1}{\rho_0} \sigma : d\epsilon \quad (2)$$

(where T_α is the absolute temperature, s is the entropy per unit mass, σ is the elastic part of the second Piola-Kirchhoff stress, ϵ is the material strain; ρ_0 is the initial reference density.)

According to the definition of heat accumulated, the rate of the change of entropy and the rate of doing work (per unit reference volume) by a linear elastic material, the following equation can be gotten [28][29]:

$$T_\alpha \rho_0 \frac{ds}{dt} = \nabla \cdot (k \nabla T_\alpha) + Q_s + \tau : \frac{d\epsilon}{dt} \quad (3)$$

(where $\frac{ds}{dt}$ the rate of change of entropy; κ is the thermal conductivity, defined in the material frame, and $\nabla \cdot (k \nabla T_\alpha)$ represents the divergence in material frame heat flux ; Q_s is the heat source per unit volume; τ is the inelastic part of the second Piola-Kirchhoff stress tensor; $\frac{d\epsilon}{dt}$ is the rate of the change of strain)

Also, by using the assumption of local equilibrium again, Maxwell relation, and Gibbs free energy, the following equation can be derived from (3) for a linearized form of the anisotropic thermoelasticity [29][30][31]:

$$\rho_0 c_p \frac{dT_\alpha}{dt} = \nabla \cdot (k \nabla T_\alpha) + \tau \frac{d\epsilon}{dt} + Q_s - T_\alpha \left[\frac{\partial \epsilon}{\partial T_\alpha} \right]_\sigma : \frac{d\sigma}{dt} \quad (4)$$

(where c_p is the heat capacity of the solid at constant stress; T_α is the absolute temperature; $\frac{d\epsilon}{dt}$ is the rate of the change of strain; Q_s is the heat source per unit volume; τ is the inelastic part of the second Piola-Kirchhoff stress tensor; and $\frac{d\sigma}{dt}$ is the rate of the change of the elastic part of stress)

This equation couples the heat transfer equation to the structural problem with an additional heat source term Q_s . The FEA tool COMSOL Multiphysics can solve a linearized form of the anisotropic thermoelasticity equations.

According to Zener's research [31], he derived an approximate analytic expression for the quality factor of a thin isotropic beam vibrating in its fundamental mode, by considering only the thermal gradients in the direction of flexure. Hence, the expression is like this [31]:

$$\frac{1}{Q} = \frac{E\alpha T_\alpha}{\rho_0 c_p} \cdot \frac{w\tau_t}{1 + (w\tau_t)^2} \quad (5)$$

(where Q is the quality factor of the mode; E is the Young's modulus of the beam, α is the isotropic thermal expansion coefficient, and ω is the mechanical angular resonant frequency; τ_t is the thermal relaxation time constant of the system based on the geometric dimensions.)

The equation (5) is based on an isotropic beam vibration, so in the research, it can be regarded as an analogy and comparison for the vibration of wineglass resonator about TED. Compared to the result data in the following result chapter of this thesis, it can be confirmed that the higher thermal expansive coefficient α can lead to a lower quality factor in the comparison between two available low expansion fused quartz such as Vycor and Fused silica.

For the resonant frequency of the beam, Zener also derived an equation about the resonant frequency for an isotropic beam [31]

$$w = 22373 \cdot \frac{t_b}{l_b^2} \sqrt{\frac{E}{12\rho_0}} \quad (6)$$

(where t_b is the beam thickness and l_b is the length of the beam; E is the elastic modulus of material; ρ_0 is the density of material)

From Equation (6), it can be observed that the high elastic modulus and lower density of material helps increase the eigenfrequency of the resonant structure, which is simulated in the following session. Equation (6) is also based on an isotropic beam vibration, but it can still be regarded as an analogy and comparison for the vibration of wineglass resonator about TED.

2.2 Geometric parameters

The design and modeling of MEMS is a unique engineering discipline. At small size scales, the design of the MEMS structures, like resonators, gyroscopes, accelerometers, and actuators, must consider the effects of several physical phenomena in their operation. COMSOL Multiphysics is used with MEMS Module to interfaces with eigenfrequency and thermoelasticity [32]. COMSOL Multiphysics was used for building the wineglass hemispherical resonator gyro, running its simulation and obtaining the relative results such as the frequency for resonant mode shape and quality factor.

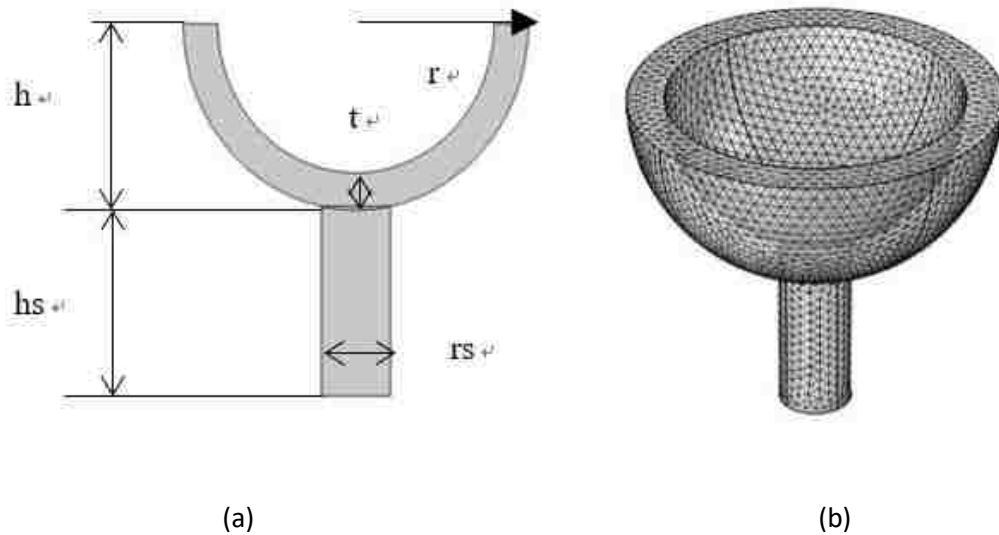
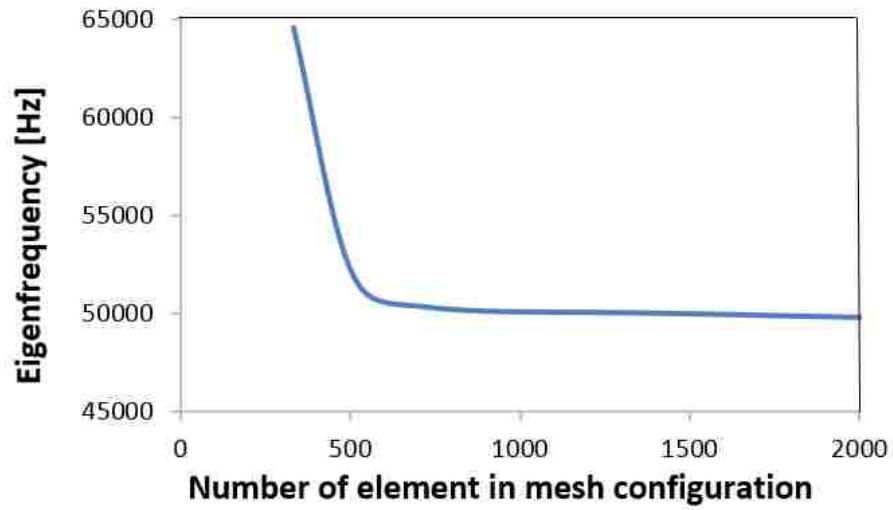


Figure 5: Schematic of showing geometric parameters and mesh configuration of resonator

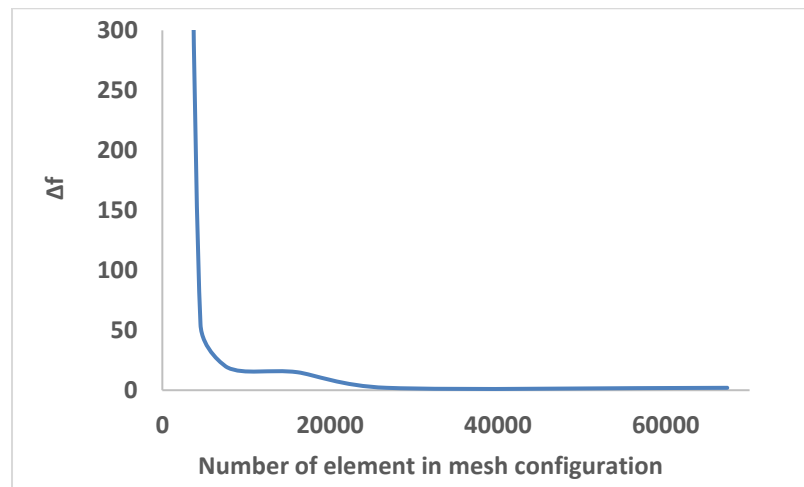
The wineglass shell model with stem was created in a 3-dimensional space (Figure 5). The size of the reference model was $h=5\text{mm}$, $t=1\text{mm}$, $r=5\text{mm}$, $r_s=1\text{mm}$, $h_s=5\text{mm}$ [32]. The reference parameters were used as the baseline for comparison and normalization because a fused silica shell resonator with the above-mentioned similar geometric parameters showed 1 million Q-factor [33]. The material properties of fused silica has a density of 2200 kg/m^3 , an elastic modulus of 73 GPa , a Poisson's ratio of 0.17 , a thermal conductivity of $1.38\text{ W/(m}\cdot\text{K)}$, a coefficient of thermal expansion of $0.55\times 10^{-7}\text{ 1/K}$, and a specific heat of $740\text{ J/(kg}\cdot\text{K)}$.

In the design interface of COMSOL, the bottom plane of the stem of the resonator was fixed. Zero temperature deviation was also applied on the bottom surface of the stem. For the physics filed, thermoelasticity was chosen, with elastic material option for the model. Then the eigenfrequency study module was used to simulate the model with searching results ranging at around 50 kHz .

2.3 Mesh Independence



(a)



(b)

Figure 6. Convergence curve showing optimum mesh configuration

Before extending the numerical experimentation, a mesh independence test was performed. The convergence curve in Figure 6 illustrates that the eigenfrequency of the

resonator converges at 4.94×10^4 Hz, when the number of elements in this mesh configuration of model is higher than the number at around 500. Thus, a mesh configuration of this resonator with 12842 elements was deemed acceptable to make sure there is no frequency split from mesh configuration as shown in Figure 6(b).

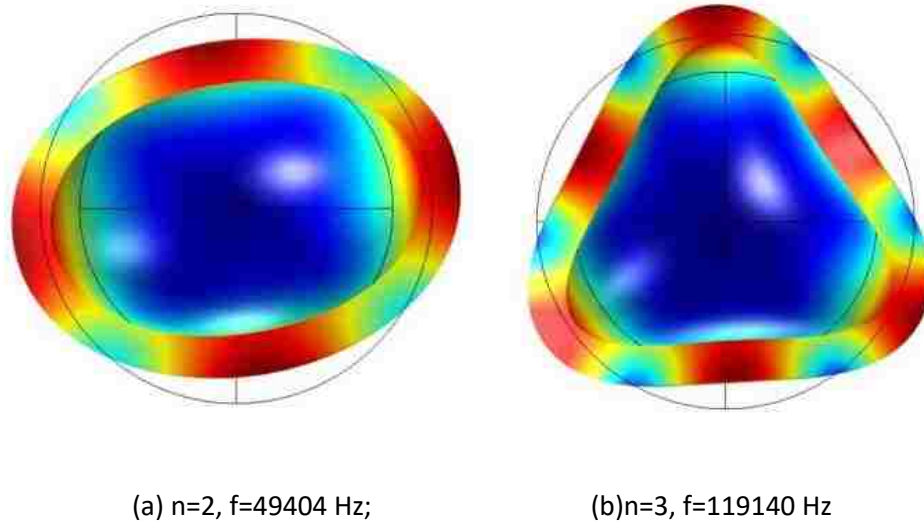


Figure 7. Surface map showing $n=2$ and $n=3$ mode shapes of the hemispherical resonator

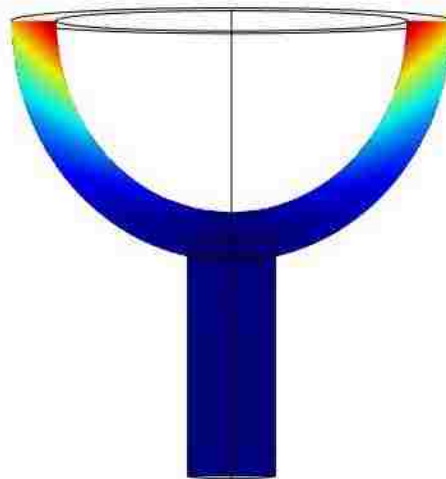


Figure 8. Cross section surface map at $n=2$ mode shape

Eigenfrequency was estimated numerically after running the simulation, the wineglass modes $n=2$ and $n=3$ were solved as shown in Figures 7 (a) and (b), respectively. The $n=2$ mode

has two degenerate mode shapes. Figure 8 is the surface displacement map from the side, showing the mode shape when $n=2$. As shown in these figures, the red parts of model represent the highest displacement during the oscillation of the devices.

2.4 Results and discussion

2.4.1 Material design

The material of the shell resonator can influence its damping performance, because thermoelastic dissipation is largely dictated by the material properties. Fused silica is widely used as a resonator material because of its lower coefficient of thermal expansion, therefore fused silica is considered as a reference material. Fused silica is an expensive but cost effective material with similar properties has long been intrigued researcher. For example, compared to fused silica, Vycor is a more cost-effective material and is equipped with comparable thermal expansion coefficient. Hence, Vycor is used to make the comparison with fused silica as the material for inertial resonator. Vycor is made of 96% silica and 4% boron trioxide. Vycor has a Young's modulus of 6.62×10^{10} Pa, a density of 2180 kg/m^3 , a Poisson's ratio of 0.19 , a thermal expansion coefficient of $7.5 \times 10^{-7} \text{ 1/K}$, a specific heat of $753.62 \text{ J/(kg}\cdot\text{K)}$, and a thermal conductivity of $1.38 \text{ W/(m}\cdot\text{K)}$. Borosilicate glass is cheaper compared to fused silica and Vycor, however its coefficient of thermal expansion is not as low as fused silica. Borosilicate glass is also tested to compare its performance.

Table 1 provides a comparison of mode shape and material properties among different reference materials, including fused silica, boron silica, and vycor. Table 2 shows that a shell resonator made of Vycor can offer us 50% of the Q factor of its Vycor counterpart when $n=2$. Obviously, the Table 2 below shows that the shell resonator can obtain a higher Q factor when it is made of fused silica. The Vycor model just shows a Q factor of 57.11% and 55.54% of the fused silica counterpart in mode $n=2$ and $n=3$ respectively.

	Fused silica	B.S.	Vycor
--	---------------------	-------------	--------------

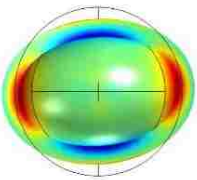
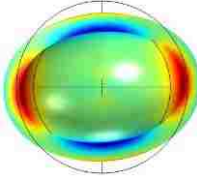
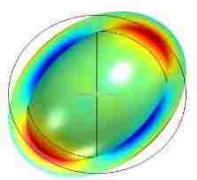
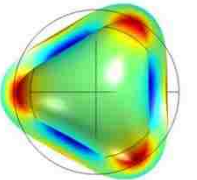
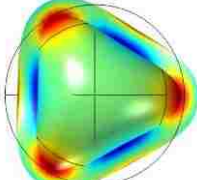
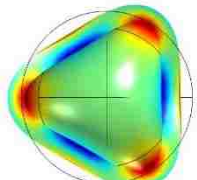
n=2	f=49403 Hz 	f=45246 Hz 	f=47259 Hz 
n=3	f=119140 Hz 	f=109370 Hz 	f=113980 Hz 
Material properties	99.99% SiO ₂	81% SiO ₂ ; 13% B ₂ O ₃ ; 4% Na ₂ O+K ₂ O; 2% Al ₂ O ₃	96% SiO ₂
Elastic modulus	7.3 x 10 ¹⁰ [Pa]	6.3 x 10 ¹⁰ [Pa]	6.62 x 10 ¹⁰ [Pa]
Density	2200 [kg/m ³]	2230 [kg/m ³]	2180 [kg/m ³]
Poisson's ratio	0.17	0.2	0.17
Coefficient of thermal expansion	5.5 x 10 ⁻⁷ [1/K]	3.3 x 10 ⁻⁶ [1/K]	7.5 x 10 ⁻⁷ [1/K]
Thermal conductivity	1.38 [W/m*K]	1.2 [W/m*K]	1.3 [W/m*K]

Table 1: Comparison of mode shape among different materials

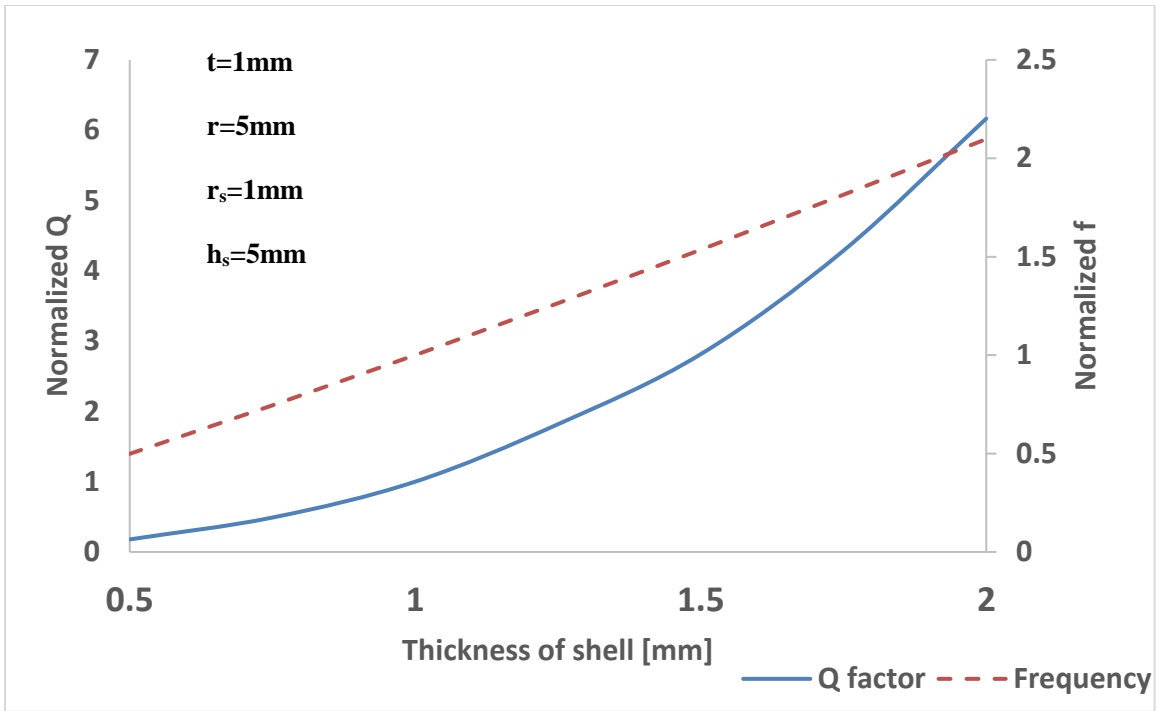
	Fused silica		B.S.		Vycor	
Mode shape	Frequency	Q factor	Frequency	Q factor	Frequency	Q factor
n=2	49401	2.04×10 ¹⁰	49401	2.05×10 ¹⁰	47022	1.17×10 ¹⁰
n=3	1.19×10 ⁵	3.24×10 ¹⁰	1.19×10 ⁵	3.21×10 ¹⁰	1.14×10 ⁵	1.80×10 ¹⁰

Table 2: Eigenfrequency and Q factor on fused silica and vycor

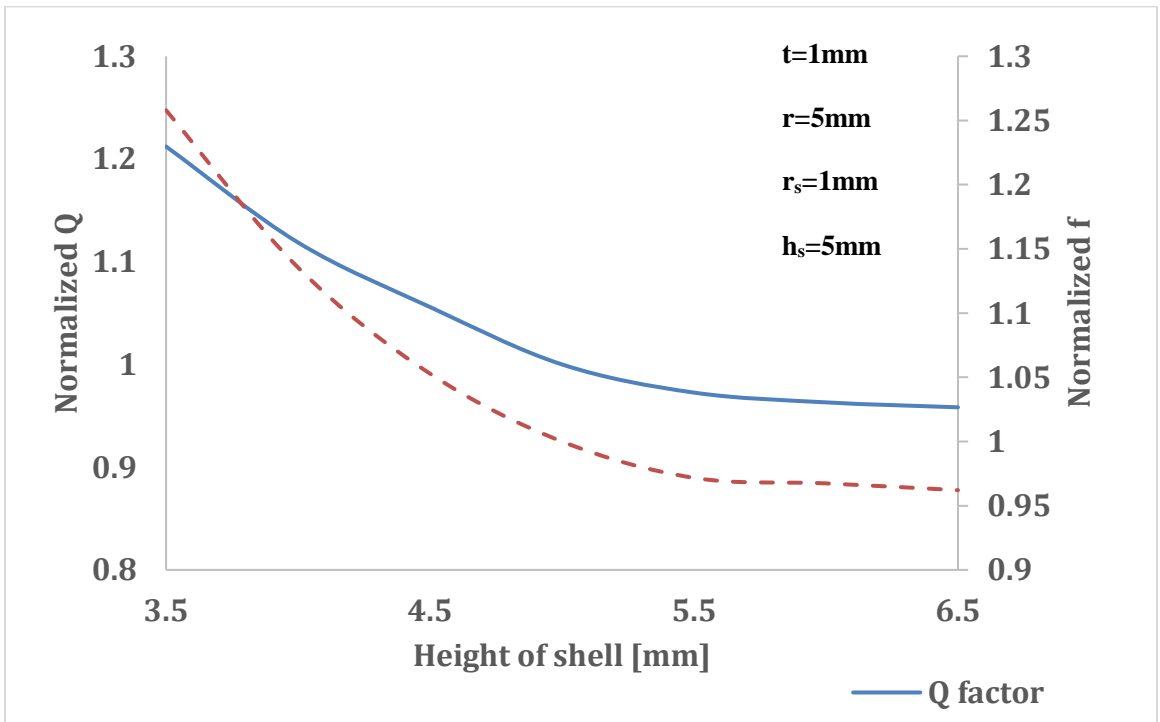
2.4.2 Geometric design

Shell geometry can influence frequency and Q factor. Changes in Q factor with respect to different geometric parameters, such as shell height, shell thickness and radius of shell were investigated. In this section, the thickness, height and radius of the shell are three variables as shown in Figure 5a. They can be readily varied to improve the performance of the wineglass hemispherical resonator. The height h of the shell is defined by the distance from the top of edge of the resonator to the stem. For the purpose of the comparison among different parameters, one property is varied at a time, while others are fixed to their sample reference size as shown in Figure 9(a).

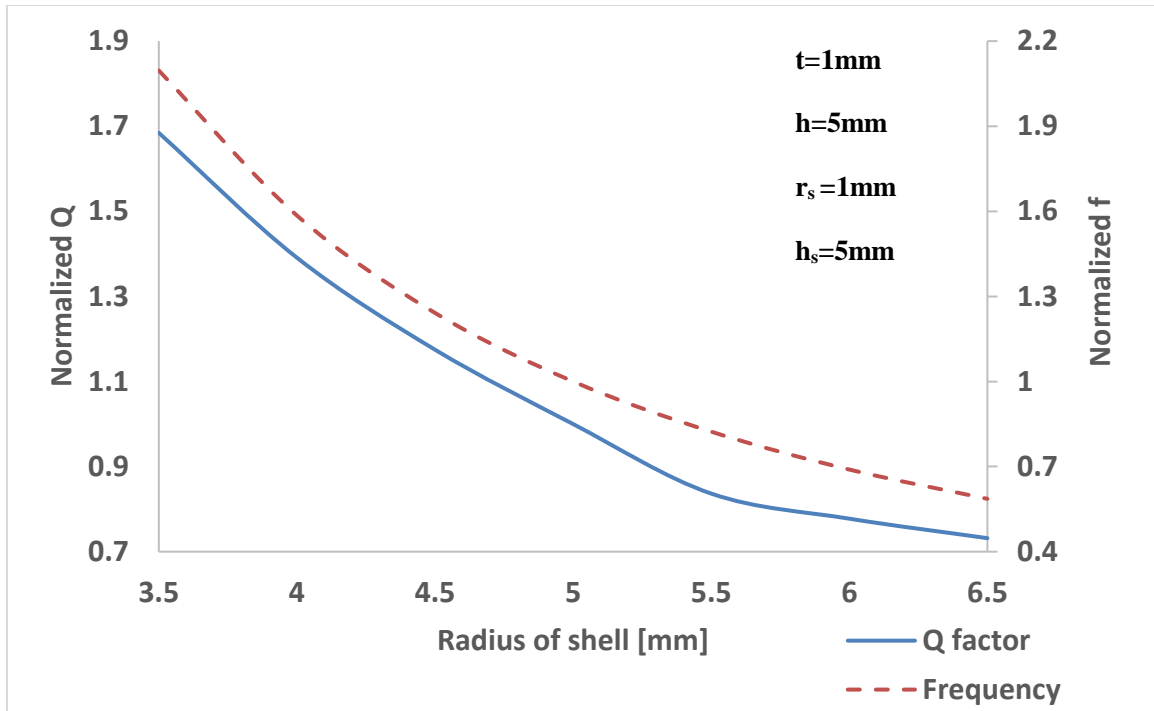
The shell thickness of the resonator is normalized with respect to the reference thickness value. The results show that when the normalized shell thickness varied from (0.5 to 2), the Q factor rises by a factor of 6, as shown in Figure 9(a). With the increase of thickness, the normalized frequency of the device is expected to double. When the normalized height and radius of the shell varies from 3.5 to 6.5 (the normalized frequency reduces from 1.25 to 1.03 and 2.1 to 0.6, respectively), there is a reduction in the Q factor as shown in Figures 9(b) and (c). These numerical simulations illustrate that raising the thickness and decreasing the shell height and the shell radius can decrease the thermoelastic damping of the resonator. However, the higher thickness increases the frequency, which may limit its operation. Hence, in order to obtain the higher Q factor, the design of the resonator should be equipped with a higher shell thickness, lower shell height, and lower shell radius. Though changing the aforementioned parameters (thickness, height, and radius) can influence the Q factor, changing only one parameter and keeping the others fixed may affect the mass of the resonator depending on which variable is varied.



(a)



(b)



(c)

Figure 9: Normalized Q and f versus (a) thickness t, (b) height h, and (c) radius r for n=2, respectively

The mass of the resonator will change by changing the geometric parameters described in the above section. The mass of the resonator can provide higher force and affect the sensitivity. The following analysis focuses on keeping the mass of the resonator fixed while changing two parameters simultaneously to observe if the Q factor can increase similarly compared with the previous results. For example, the ratio of thickness and height (t/h) can be changed at the same time, while keeping the volume of resonator fixed. As shown in Figure 10, the variation of the Q factor shows the set of results similar with the previous section when only one parameter was varied. This implies that the small amount of change in mass [or volume] will not produce a noticeable change for Q factor.

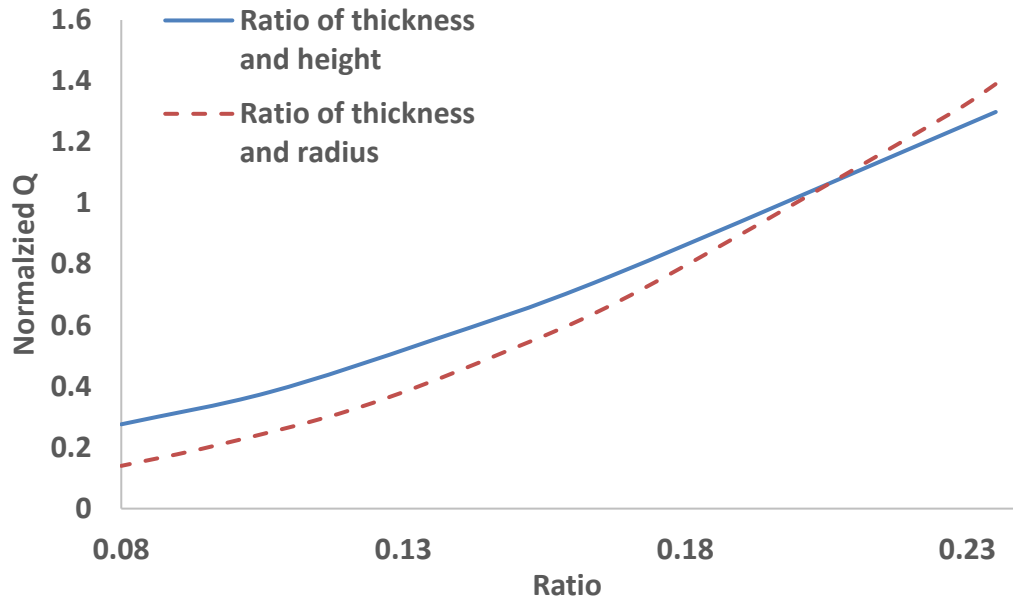
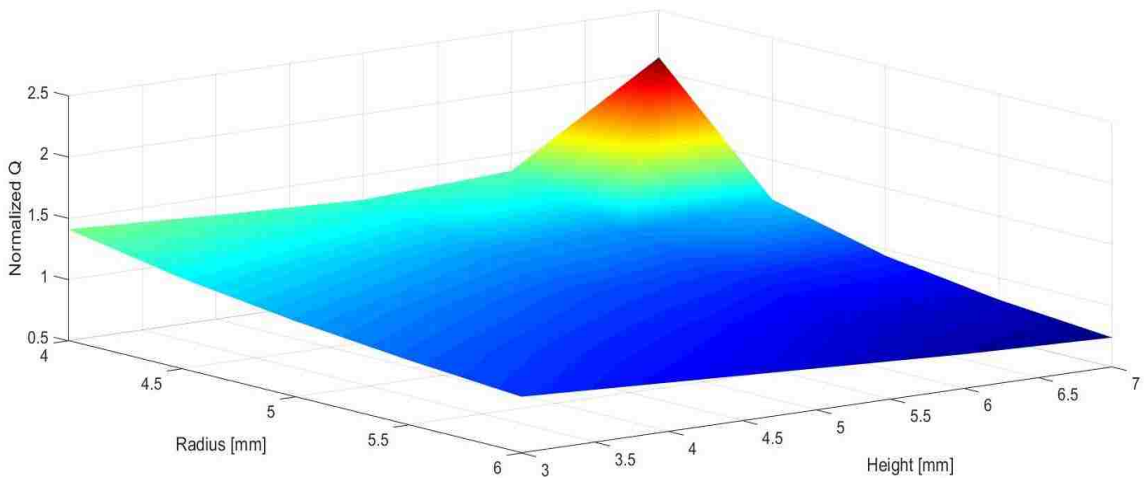
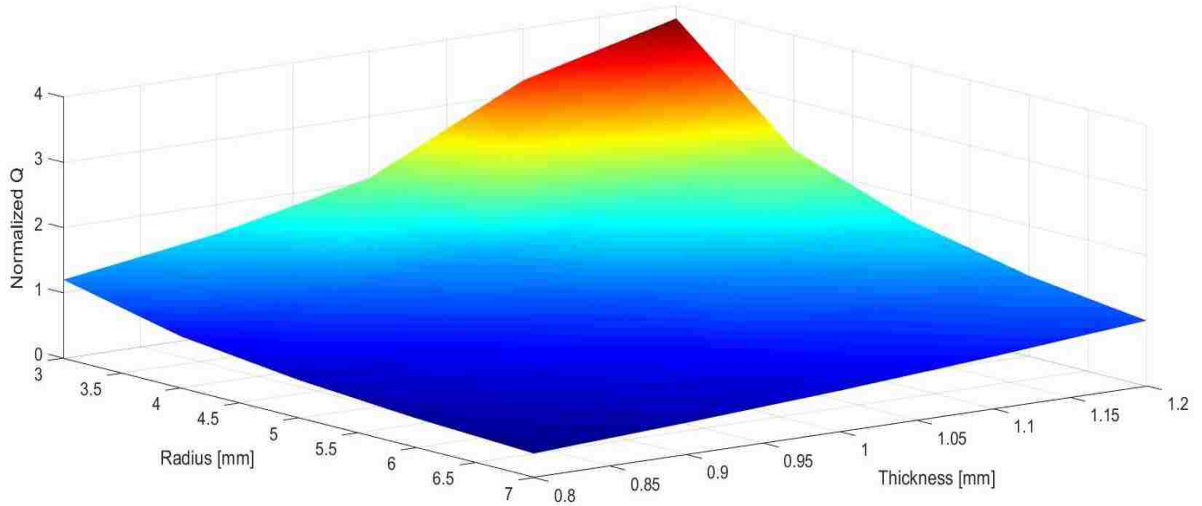


Figure 10: Normalized Q versus the ratio of (a) t/h and (b) t/r respectively for $n=2$.

Figure 11 (a) clearly shows that the higher normalized Q (approximately 3) is obtained when the lower radius and the higher height of shell are taken but keeping thickness as 1mm. Also, Figure 11 (b) illustrates that higher Q value exists in the combination among the dimensions of lower shell and higher thickness but keeping the height of shell as 5 mm.



(a)



(b)

Figure 11 : (a) 3D graph showing Q factor with radius and height of shell

(b) 3D graph showing Q factor with radius and height of shell

2.4.3 Geometric non-uniformity

2.4.3.1 Effect of shell non-uniformity

Non-uniformity in the shell thickness, which includes a thinner or thicker inner shell, can be created during fabrication (Figure 12). Non-uniformity may affect the frequency and Q factor of the resonator. In the design, the non-uniformity is created by the difference in thickness between the outer and inner radius at the location in Figure 12 is defined as A . In this case, the width of the thin edge A was analyzed. The other parameters were kept constant ($t=1\text{ mm}$, $h=5\text{ mm}$, $r=5\text{ mm}$, $r_s=5\text{ mm}$, $h_s=5\text{ mm}$).

The width of thin edge A is varied from 0.2 mm to 0.8 mm when the normalized frequency was expected to change from 2.5 to 0.2 . The results taken from the simulation illustrates that the Q factor rises by the factor of 2.58 when A is reduced to 0.2 mm . It demonstrates that a high Q factor exists by designing a thinner edge under the non-uniformity shell resonator as shown in Figure 13.

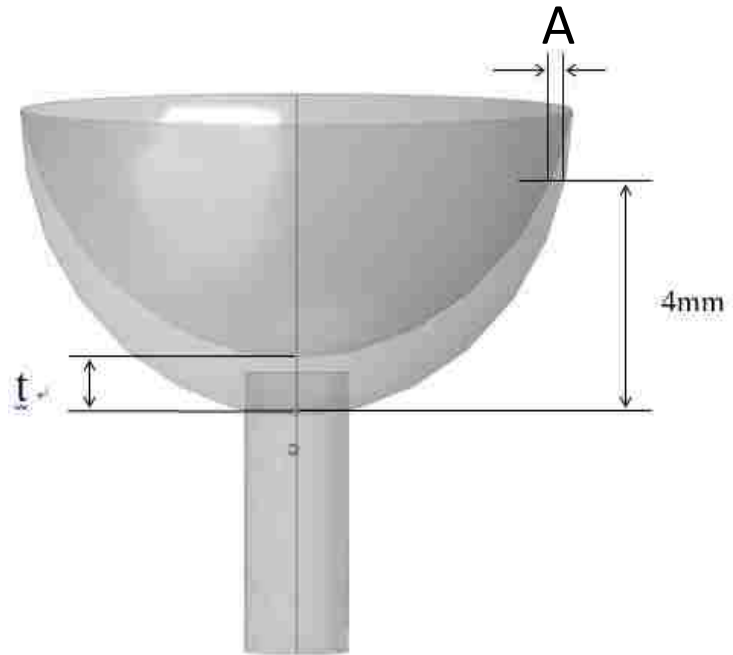


Figure 12: Schematic dimensions for non-uniformity in thickness of a resonator

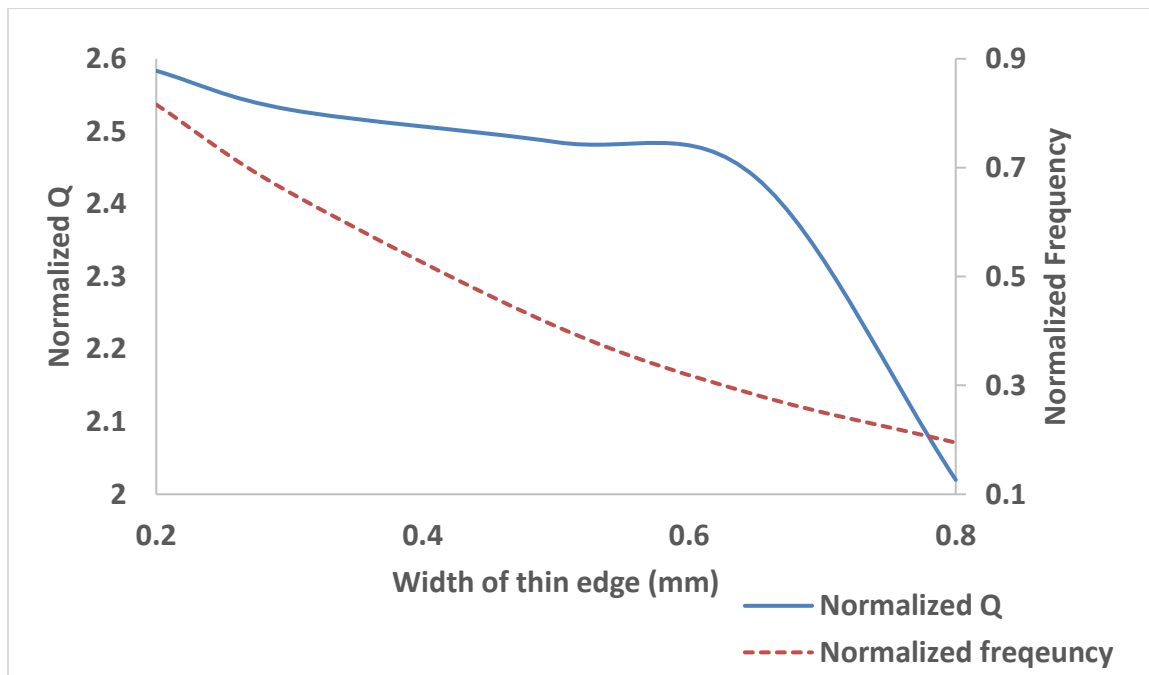


Figure 13: Normalized Q versus the thin edge of the non-uniformity resonator

2.4.3.2 Effect of gravity center

The stem of the resonator needs to be at the center of the shell in order to create frequency symmetry between the degenerate modes. Due to misalignment during fabrication, the center of the stem may shift and create asymmetry and mass imbalance. Therefore, the important aspect to consideration is the gravity center of a resonator with a stem. The center of mass for the resonator varies when the stem does not align with the center point of the shell. Misalignment can occur during fabrication of the mask alignment. The following analysis focuses on how the Q factor varies due to the stem misalignment from the original location (center at the base of the shell). Figure 14 shows a relationship between the normalized Q and the offset, as well as the frequency and the offset, respectively, depending on the variation of radius of the shell ($R=5\text{mm}$, 5.5mm and 6mm , respectively).

Figure 14 shows that the misalignment varies up to 2 mm . The corresponding change of frequency, which reduces from 49.4 kHz to 46.7 kHz ($R=5\text{mm}$), was not significant. However as shown in Figure 14, the significant rise of the Q factor can be obtained when the stem offset moves closer to the original point, which means that breaking the symmetry can drastically increase the TED loss mechanism in the device.

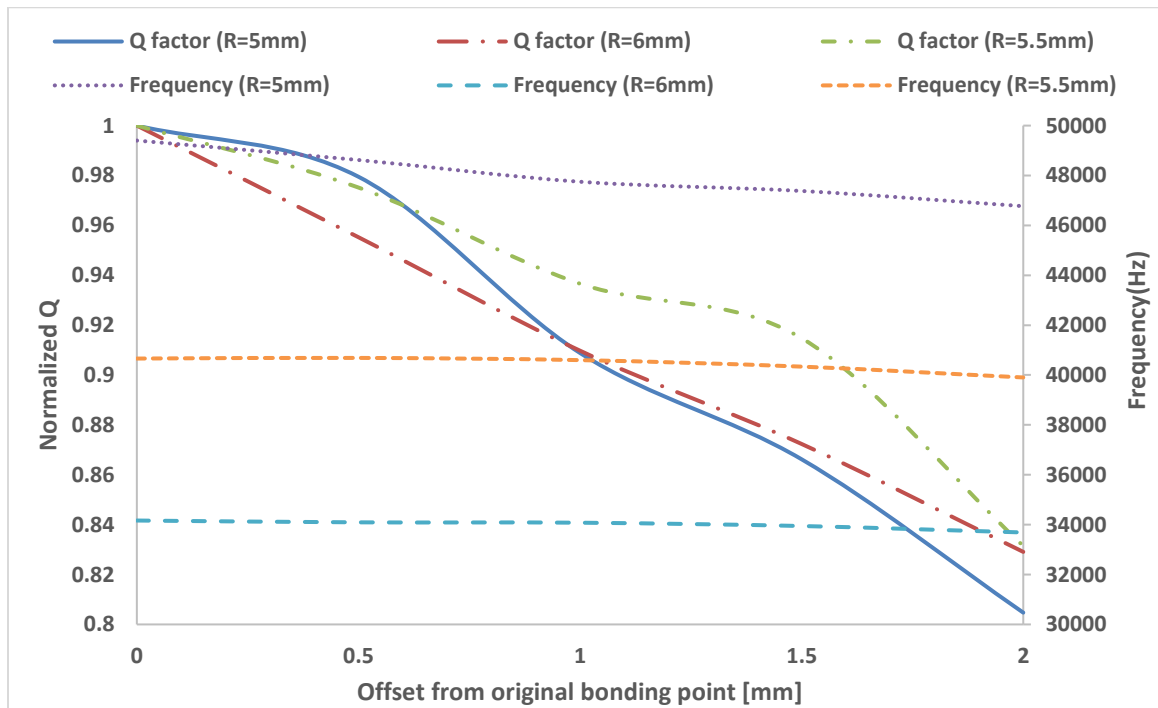


Figure 14: Normalized Q factor and frequency versus stem offset from original symmetry point for $n=2$

2.4.4 Effect of fabrication inaccuracy

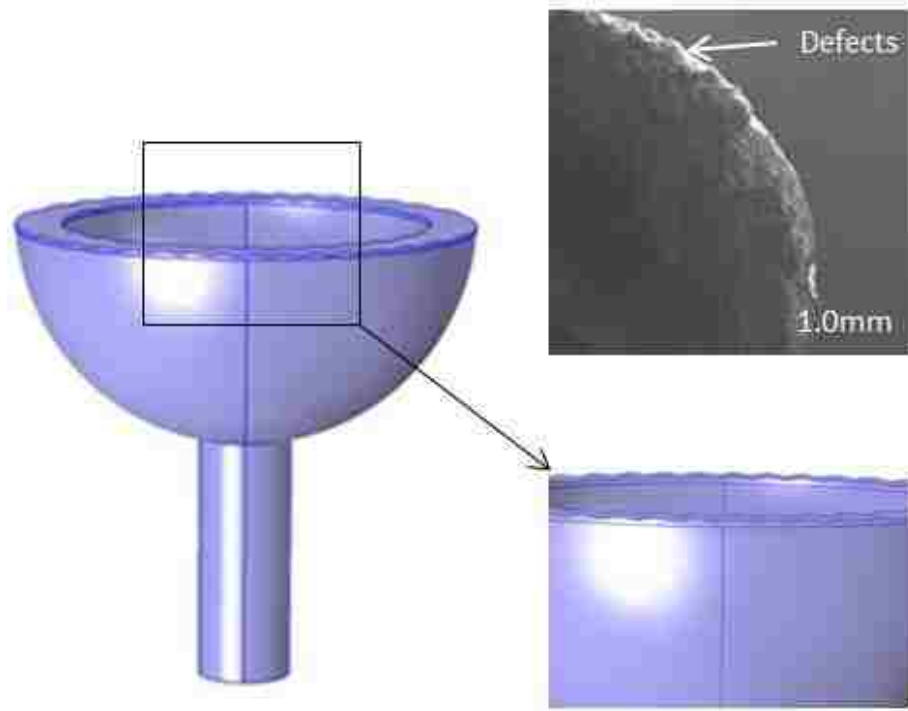


Figure 15: SEM image shows defects along the edge due to fabrication and the model used in simulating defected surface.

This section investigates how the edge defects on the surface affect the performance of the resonator. The fabrication process causes undesirable and unavoidable defects at the edge during the releasing of the outer shell edge. A SEM image of the edge of fabricated device is shown in Figure 15. The figure demonstrates a severe scenario of edge defects. Hence, the amount of energy dissipation created by the defects on edge must be taken into consideration. In the simulation process, random curved surfaces were utilized on the model to simulate the irregularities on the edge of the resonators.

Effect of edge defects was simulated by replacing it with random sinusoidal surface on the surface of the resonator. The results obtained illustrate that Q factor reduced significantly (40%) when the normalized amplitude of sinusoid curve surface varies from 0.5 to 5 as shown in Figure 16, with the decrease of frequency as well.

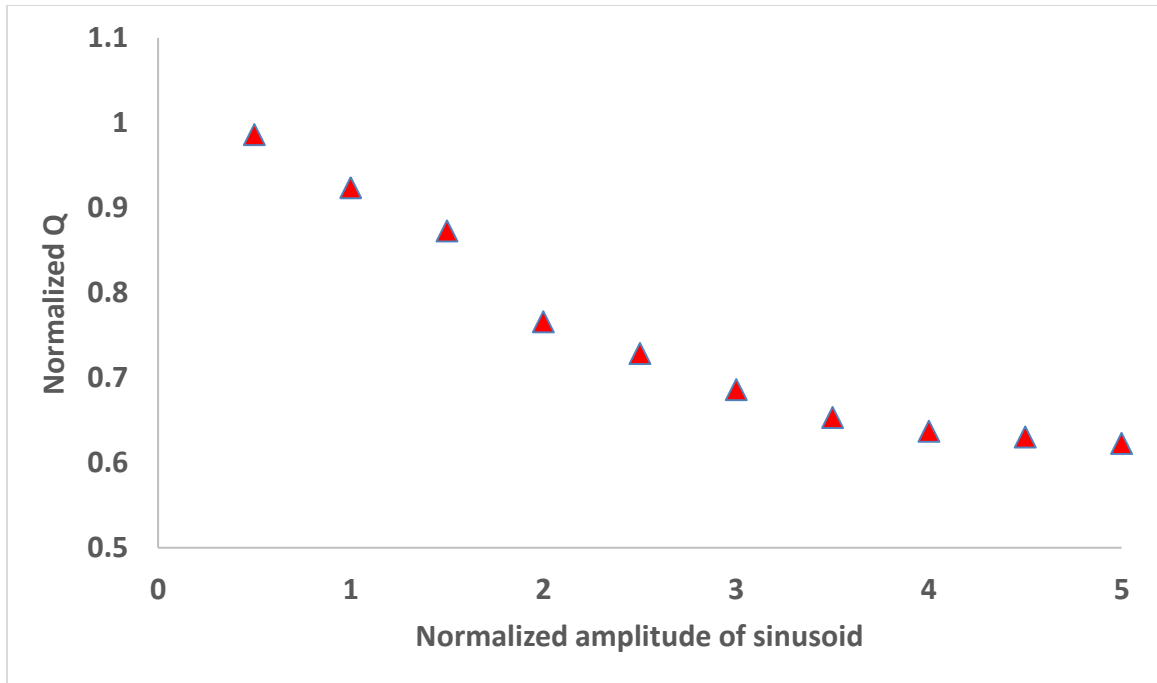


Figure 16: Normalized Q factor (n=2) versus normalized defect parameters simulated with random curved surfaces.

2.5 Conclusion

The above content numerically analyzes the thermoelastic damping on the Q factor of the shell resonators for different geometric and material properties. The results obtained indicate that the Q factor tends to increase to a factor of 6 when the normalized thickness of the shell increases by two folds. Furthermore, non-uniformity in shell thickness can be effectively manipulated to enhance the Q-factor. Glassblowing techniques can produce non-uniform shell thickness. The results obtained show that non-uniformity with thinner edge (0.2 times that of edge thickness) increases the Q factor by 2.58 times. Eccentricity in the center of gravity, which may happen during fabrication misalignment, can drastically reduce the Q. Different resonator materials were analyzed, among the different materials available; the cost effective ones, such as Vycor, can offer about half of the Q factor of fused silica. Moreover, edge defects can reduce Q-factor. Irregular curved surfaces on resonators are proven to decrease the Q factor by a large factor. The results obtained show that the Q factor of the resonator with sinusoidal curved surfaces reduces by 38% when the normalized amplitude of sinusoid curved surface increases to a factor of 5. The model presented above can be used for optimized design of 3D shell resonator

for high Q-factor and low damping. Minimizing the thermoelastic dissipation in the energy loss is critical to the development of MEMS HRG with high precision.

Chapter 3: Energy loss in disc resonator gyro

3.1 Introduction

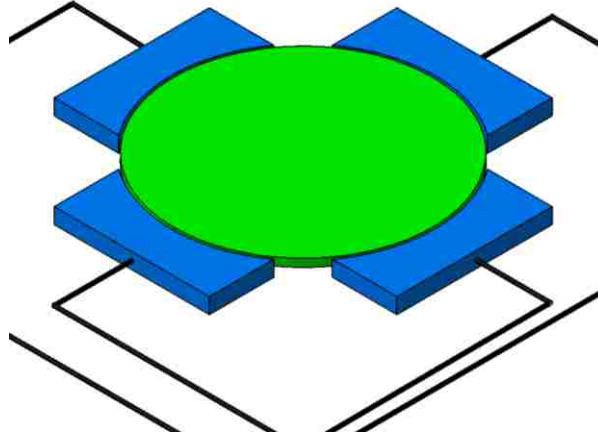


Figure 17: Perspective view schematic of an MEMS disk resonator illustrating excitation scheme

The previous chapter investigated the hemispherical shape resonator. In this chapter, disk shape resonator is analyzed. Both the disk and hemisphere have the same mode shape and similar vibration characteristics. However, disk resonator can be fabricated using conventional microfabrication techniques compared to customized techniques for hemisphere fabrication. Therefore, the goal was to compare both geometries and extend the understanding by expanding the loss mechanism analysis with other dynamic effects such as squeeze film damping and anchor loss into the mode.

Figure 17 presents the perspective-view schematic of the disk resonator, identifying the key components. The resonator consists of a disk suspended $500 \text{ } \mu\text{m}$ radius with a single anchor at its center. Four conformal input electrodes surround the perimeter of the disk. They are separated from the disk by a small air gap. This small gap defines the capacitive and electromechanical transducer. When the input signal is acting at the resonant frequency of the resonator, the effect of that force is multiplied by the quality factor of the resonator, producing expansion and contraction of the disk along its radius, as shown in Figure 19 (a), which illustrates the shape of the fundamental mode [34]. Hence, the motion creates a time-varying and dc-biased capacitor between the disk and the output electrode, which generates an output current as [34]:

$$i_0 = V_p \cdot \frac{\partial C_0}{\partial r} \frac{\partial r}{\partial t} \quad (10)$$

(where r is the radial displacement at the edge of the disk and $\frac{\partial C_0}{\partial r}$ is the change in electrode-to-resonator sense capacitance per unit displacement, and V_p is the dc bias voltage)

In terms of the mechanical resonant frequency for the radial contour mode of a disk, Clark et al. presented that the resonant frequency is governed mainly by its material properties and its radius [34]. So the equation of frequency can be rendered to a more intuitive form as [34]:

$$\omega = \frac{k\alpha}{r} \sqrt{\frac{E}{\rho}} \quad (11)$$

(where k is a parameter dependent upon Poisson's ratio, α depends on the desired mode, E is the elastic modulus, and ρ is the density of the material of the disc)

The numerical model represents the electric potential. The necessary transformations are taken care of by the electro-mechanic interface, which also contains smoothing equations about the movement of the mesh in the air domain.

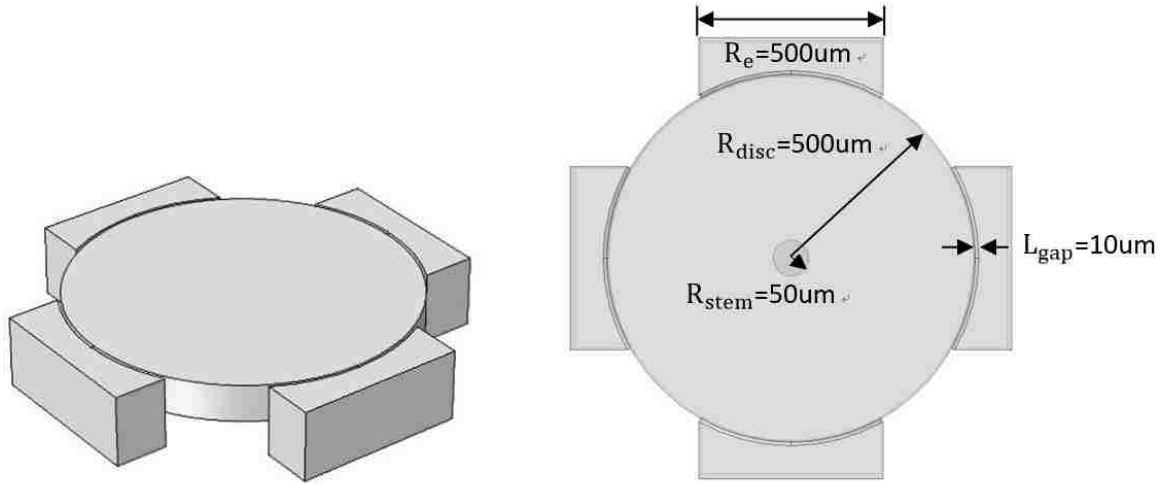
For the oscillation of a disc resonator, the main output parameter is the displacement of the mechanical model. This variable is equivalent to the radial displacement at the perimeter of the mode shape of disc along its radius [34]. According to [34] the amplitude of displacement on the disc is shown as

$$R = \frac{QC_0V_pV_i}{g_0k_{re}} \quad (12)$$

(where V_i is the amplitude of the ac input signal at the frequency, V_p is the dc bias voltage, V_i the amplitude of the ac input signal at the disk resonant frequency, g_0 is the gap between electrodes and disc resonator, C_0 is the static electrode-to-resonator capacitance at the input port, and k_{re} is the effective stiffness at the perimeter of the disk resonator.)

3.2 Geometric parameters

3.2.1 Finite element modeling



(a) Perspective-view schematic of the model. (b) Dimensions of the COMSOL model

Figure 18: 3D model about disc resonator with four conformal electrodes in COMSOL

As shown in Figure 18, the model presents the perspective-view schematic of the subject disk resonator in four typical electrodes, including the key parts and dimensions. In the figure, this device consists of a fused silica disk with $500\mu\text{m}$ radius, suspended above the substrate by a centrally located, self-aligned stem with $100\mu\text{m}$ height and $50\mu\text{m}$ radius, and surrounded by four polysilicon electrodes spaced at around $10\mu\text{m}$ from its perimeter. The space gap can be applied to drive electro-statically the device into a resonance mode shape where it expands and contracts around its perimeter. The bottom surface of the stem of the disc and the electrodes are set to a fixed constraint. The electrodes are doped, so that electric field penetration into the structure can be neglected. The disc is put in an air-filled and electrically insulated chamber. The right side electrode is a positive terminal with potential, but the left side electrode is equipped with zero voltage as terminal. The model is symmetric on the XY-plane at the plane $z = 0$. The edge of the disc is set to be a grounded electrode, which represents the grounded substrate. The model has $100\mu\text{m}$ of free air above and below the sides of the disc, while the gap between the disc and electrodes is set to be $10\mu\text{m}$ like my original model.

In my model, I used the Electro-mechanics interface of COMSOL Multiphysics to simulate the process of the disc resonator gyroscope. An electrostatic force is caused by an applied potential difference between the two electrodes. The disc oscillates when it is activated by the

setting potential on electrodes. A part of the disc's edge is bent up and down. To compute the electrostatic force, the model was calculated by the electric field in the surrounding air. The model was simulated including a layer of air 100 μm thick to the above and to the bottom plane of air and the air gap between the disc and conformal electrodes (10 μm). As the disc suffers vibration, the geometry of the air gap continuously varied, resulting in a difference in the electric field between the input and output electrodes. Hence, these coupled physics are calculated automatically by the Electro-mechanics interface in COMSOL Multiphysics. For the gyroscope model in this research, the presence of a thin gap between the disc and electrodes increases the amount of damping considerably. When the disc oscillates, it squeezes the gap and the gas flows out from the gap [34]. The narrow gap space restricts the flow causing the gas pressure to increase [34].

After the simulation is done, the mode shape of the model can be obtained as shown in Figure 19 (b). The mode shape is equipped with four nodal points that represent the maximum displacement when it is in oscillation. Figure 19 (c) is the cross section screen taken from the mode shape on $y=0$ (x - z plane).

[34]

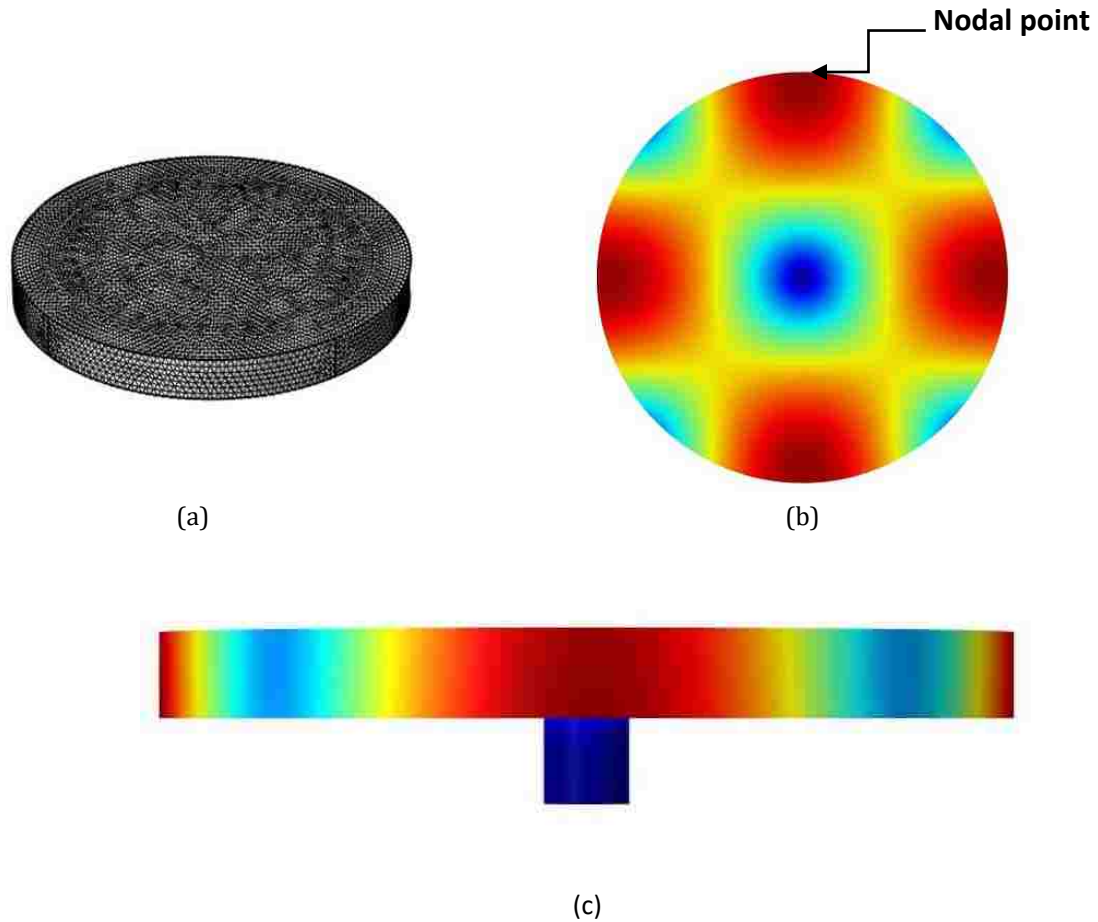
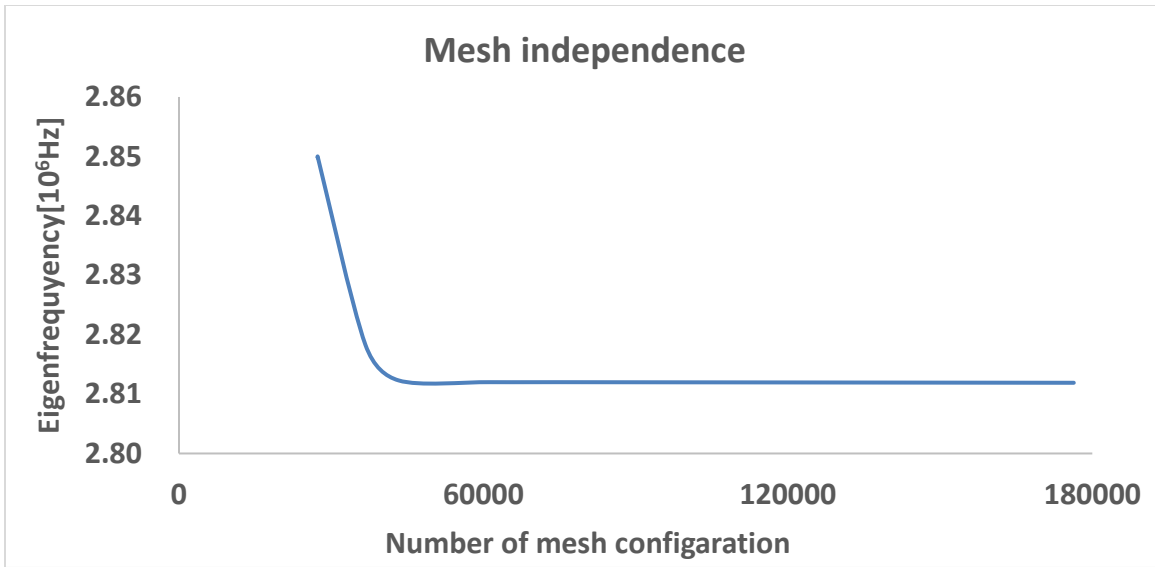


Figure 19: (a) Mesh configuration on the disc resonator model.
 (b) Surface map showing mode shape (n=2) of the resonator in COMSOL
 (c) Cross section surface plot at the of the n=2 mode shape

3.2.2 Mesh independence test

The convergence curve in Figure 20 illustrates that the eigenfrequency of the disc resonator gyro converges at $2.8119 \times 10^6 \text{ Hz}$. Thus, a mesh configuration of this resonator with 74425 elements (Figure 19 (a)) was deemed acceptable. Here the disc with finer mesh grids can be set, which can get the results closer to a real situation. However, it can also lead to a longer simulation time.



(a)

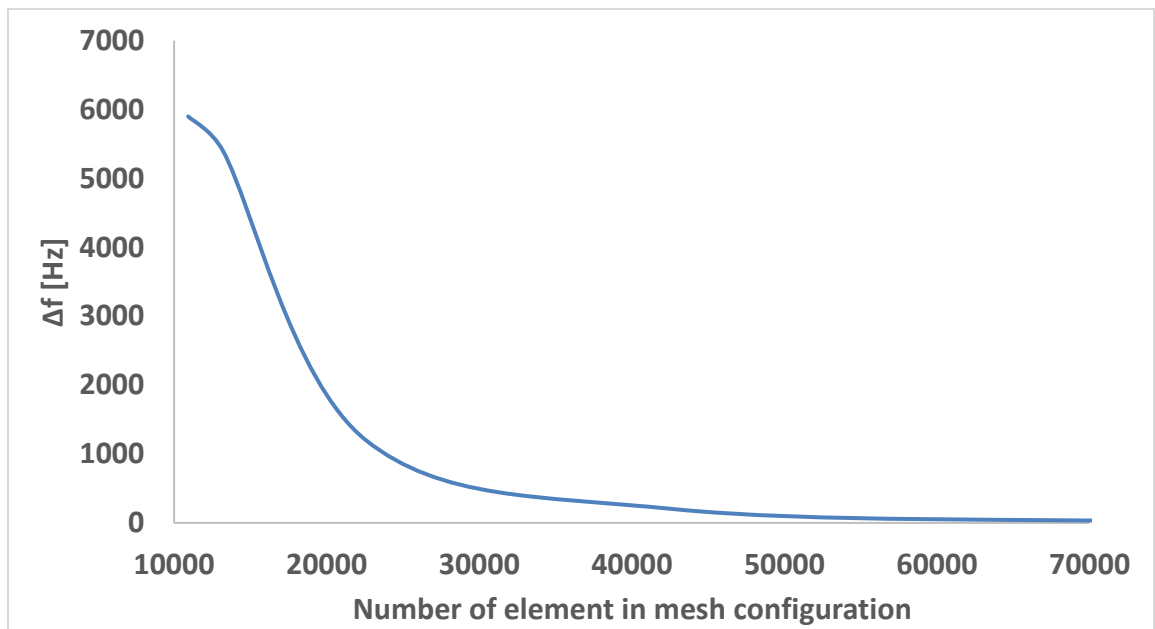


Figure 20: Convergence curve showing optimum mesh for the disk resonator model.

3.3 Results and discussion

The results of the simulation from the model are presented in the following sections. At first, a parametric study was performed to understand the role of some key design parameters of materials on the Q factor. Secondly, different dimensions of the disc were investigated comprehensively, including its radius and thickness. Next, the gap between the disc and

electrodes was analyzed to achieve a high Q. Finally, the non-uniformity shape of a disc like an ellipse was simulated to see how it would affect the performance of the disc resonator.

3.3.1 Effect of material properties

A material for a disc resonator can influence its performance a lot, because thermo-elastic dissipation has a close relation with the material properties, which is like the case for HRG.

In the next several simulation cases, fused silica was used as the reference material because Reference [1] shows that a fused silica shell resonator with similar geometric parameters produced a 1-million Q-factor. It is believed that this material can also be used to create the high Q factor and low damping for disc resonators. The material properties of fused silica have a density of 2200 kg/m^3 , an elastic modulus of 73 GPa , a Poisson's ratio of 0.17 , a thermal conductivity of $1.38 \text{ W/(m}\cdot\text{K)}$, a coefficient of thermal expansion of $0.55 \cdot 10^{-7} \text{ 1/K}$, and a specific heat of $740 \text{ J/(kg}\cdot\text{K)}$.

Compared with fused silica, there are several materials available for disc resonators, so it is important to define which property in these materials has an effect on energy dissipation.

<i>Young's modulus[GPa]</i>	<i>Frequency [10^6Hz]</i>	<i>Normalized Q</i>	<i>Normalized displacement</i>
73	2.810	1.000	1.000
63	2.610	0.929	0.622
53	2.390	0.850	0.034
43	2.150	0.765	0.025
33	1.890	0.673	0.120

Table 3: Frequency and normalized Q versus Young's modulus respectively when $n=4$

Clearly, Table 3 above shows that the disc resonator gyroscope can obtain higher frequency and Q factor when the material is equipped with higher Young's modulus under $n=4$ mode shape. The quality factor of disc gyro is 1.4 times of the original one when the Young's modulus doubles. It implies that the increase of Young's modulus enhances the coupling between the mechanical and thermal regions, which results in higher Q factor.

<i>Density[kg/m³]</i>	<i>Frequency [10⁶Hz]</i>	<i>Normalized Q</i>
2200	2.810	1.000
2100	2.870	1.021
2000	2.930	1.043
1900	2.990	1.064
1800	3.050	1.085
1700	3.110	1.107

Table 4: Frequency and normalized Q versus density of material respectively when n=4

Table 4 also shows the relation among the frequency of material, Q factor and the density of disc material. Simulation results obtained illustrate that the frequency tends to increase slightly with the lower density of material. Moreover, the Q factor rises slightly (about 1.1 times) when the density becomes smaller (from 2200 to 1700kg/m³). It means that a lower density of material can reduce the energy dissipation, which helps obtain the higher Q factor during the disc's oscillation.

<i>Poisson's ratio</i>	<i>Frequency [10⁶Hz]</i>	<i>Normalized Q</i>	<i>Normalized displacement</i>
0.17	2.810	1.000	1.000
0.19	2.780	0.989	0.134
0.21	2.760	0.982	0.072
0.23	2.742	0.976	0.033
0.25	2.720	0.968	0.007

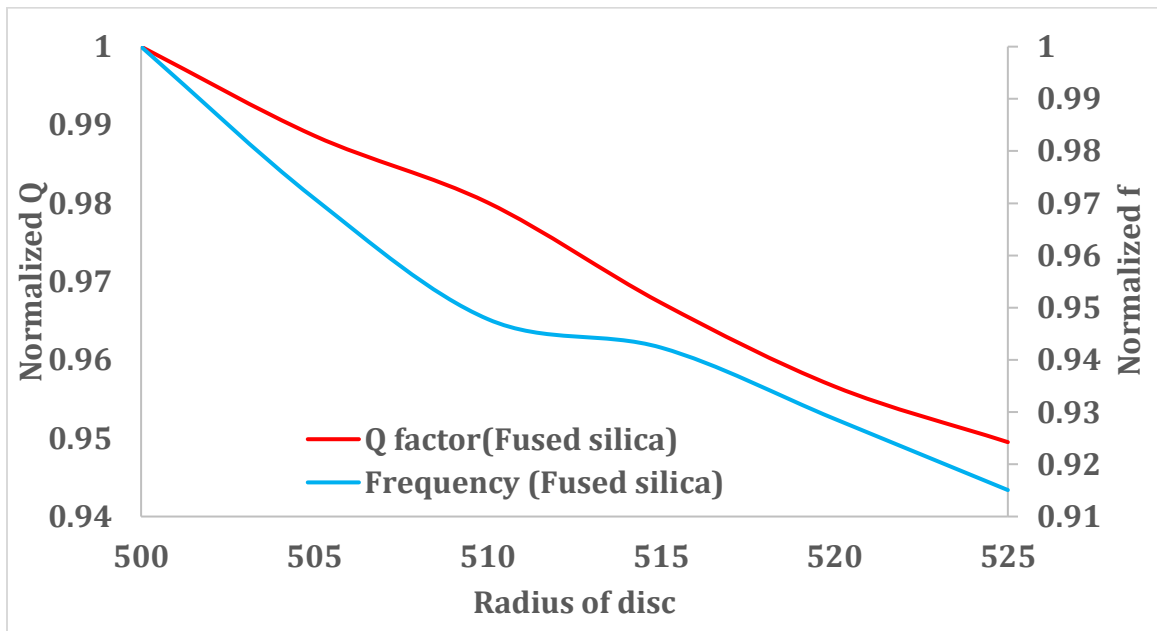
Table 5: Frequency and normalized Q versus *Poisson's ratio* of material respectively when n=4

Table 5 shows an obvious decreasing trend for *Poisson's ratio* of disc material for both frequency (from 2.81 to 2.72·10⁶Hz), normalized Q factor (from 1 to 0.968) and when the *Poisson's ratio* rises (from 0.17 to 0.25). The normalized displacement of the edge of disc also met a drastically drop to 0.007. It means a lower *Poisson's ratio* of a material can help obtain a higher quality factor.

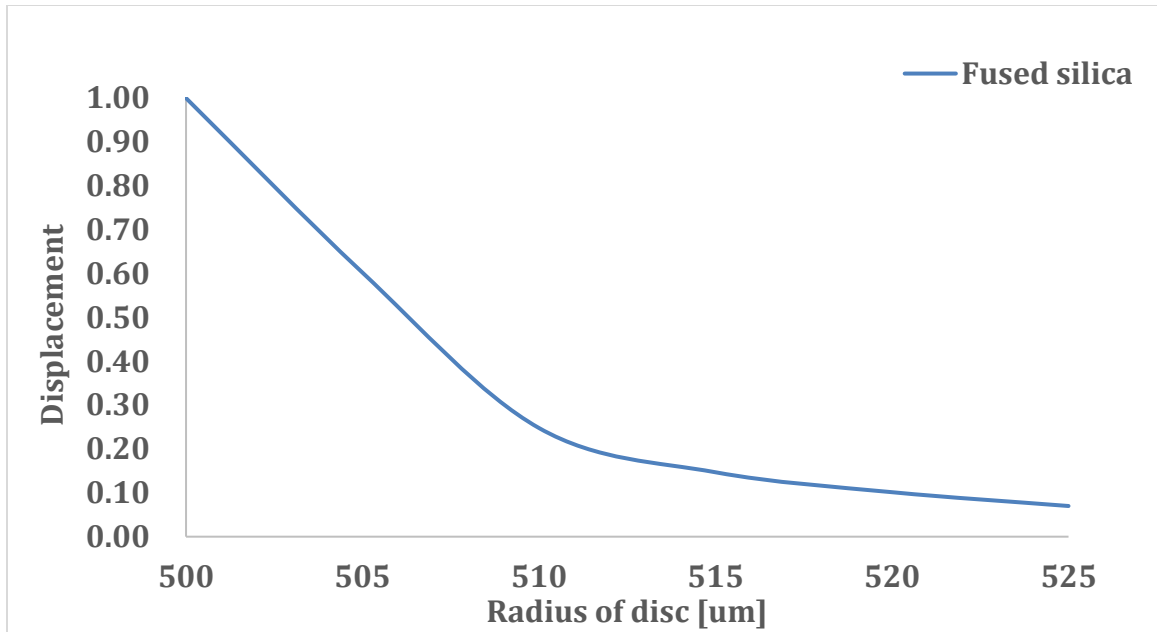
3.3.2 Effect of disc radius

Radius of the disk is varied while keeping other parameters constant. The following two figures of the results by COMSOL clearly show that the frequency and Q factor decreases

significantly with the increase of radius of disc as shown in Figure 21 (a). Figure 21(b) clearly illustrates that the higher displacement (around 10 times) of disc during oscillation occurs when the radius is reduced from 525 μm to 500 μm for fused silica. These numerical simulations illustrate that the larger radius of disc can increase the energy damping of the resonator. Hence, the higher Q factor can be obtained when the design of resonator is equipped with a smaller radius disc.



(a)



(b)

Figure 21: Normalized frequency, Q, and displacement versus disc diameter respectively when $n=4$

3.3.3 Effect of disc thickness

In this section, the thickness is varied to observe if it affects the performance of the model during simulation. Figure 22 shows the relationship between the frequency and normalized Q with the difference of disc thickness. In the simulation, when the thickness of disc was doubled, the normalized Q tends to increase substantially (from 0.65 to 1). It also shows that the normalized displacement can drastically increase from 0.03 to 1 for the resonator which was made of fused silica.

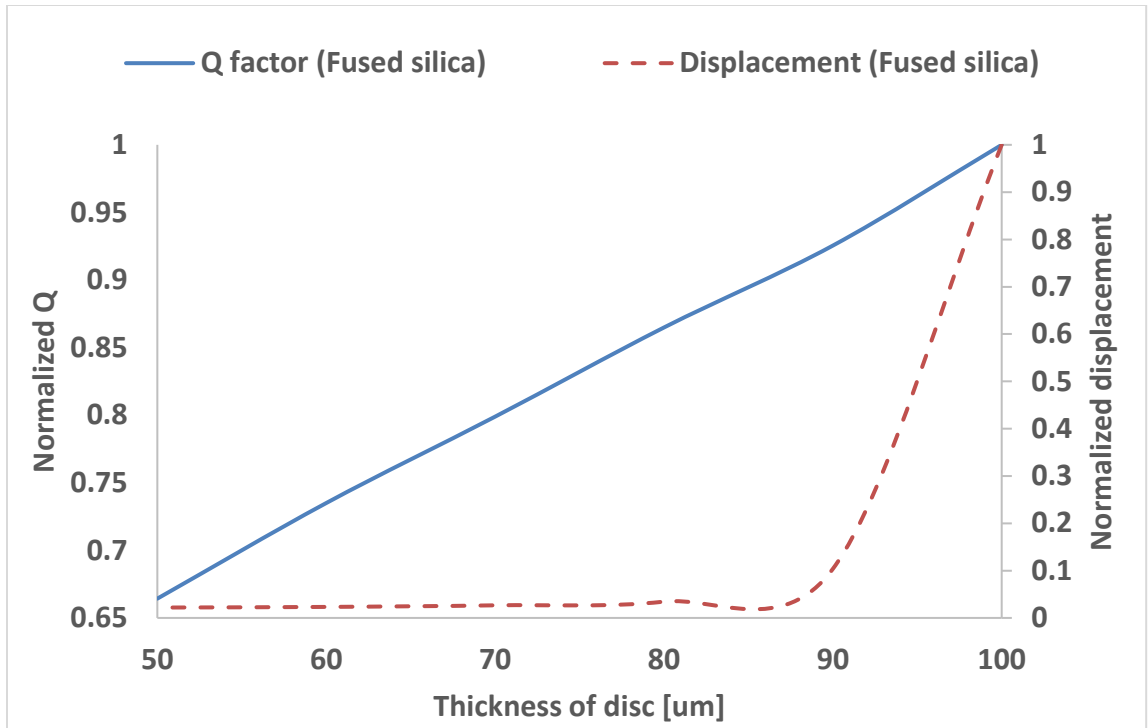


Figure 22: Normalized Q and displacement versus disc thickness respectively when $n=4$

As the discussion above, different parameters of shell resonator influence the Q factor to some extent. However, changing one parameter while keeping the others fixed affect the mass of disc as well. Hence, whether the mass (or volume) difference affects the Q factor deserves to be considered. According to the results in Chapter 2, the difference of one parameter for the hemispherical wineglass resonator (other parameters are the same) may affect the mass or volume of the model, but it would not influence the simulation results. Because of the similar mode for the HRG and DRG model in my thesis, here I believe that this result can also be applied in the DRG model. This means that the difference of volume or mass does not affect the results presented in Chapters 3.3.2 and 3.3.3.

3.3.4 Effect of gap

The critical parts of disc gyroscope are the disc with stem and conformal electrodes. As shown in Figure 18 (b), there is a gap existing between the disc and the electrodes. The purpose of this gap is to ensure that there is enough space for the disc when it suffers radial vibration

and electric- statically drive the disc into resonant mode shape when it is activated by alternative voltage. To improve the Q of disc resonator gyroscope, the model was simulated on to find out how to define the gap value. Normally the gap is at least 0.01 times higher than the disc diameter, so the gap of simulation was set to range from $10\ \mu\text{m}$ to $35\ \mu\text{m}$.

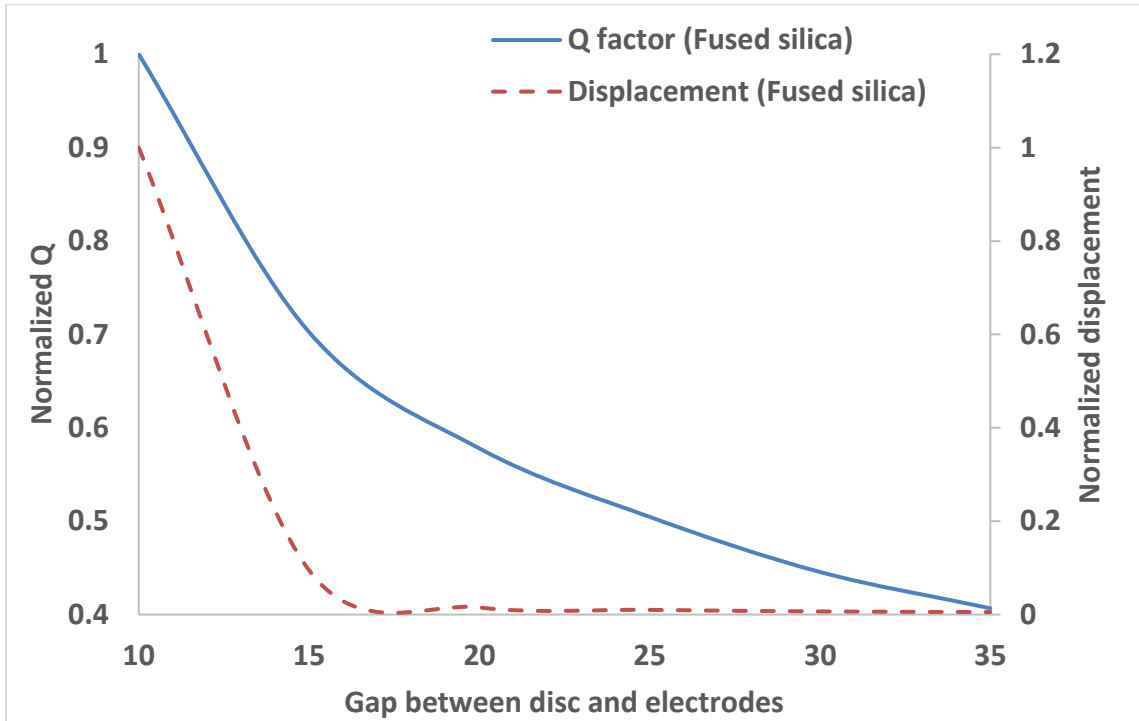


Figure 23: Normalized Q and displacement versus disc thickness respectively when $n=4$

The results obtained from the simulation show that the frequency of DRG remained the same, when the gap increases. It means that its frequency was not affected by the gap value. However, Figure 23 illustrates that the Q value drops by 60% if the gap value increases from $10\ \mu\text{m}$ to $35\ \mu\text{m}$, if the disc is made of fused silica. It is because the bigger gap creates the higher impedance for the energy excitation from disc edges to the electrodes. Hence, the smaller gap between the disc and electrodes could help obtain the high Q factor in the DRG. This figure also illustrates that the displacement shares the same decreasing relationship with the increase of gap value.

3.3.5 Effect of ellipse disc

An effect of non-uniformity shape of disc is analyzed, such as ellipse in 2D with the sample dimensions. In this section, an ellipse disc aligned with stem and surrounded by conformal electrodes was created for the simulation. Here I would analyze how the value of the semi-major axis of the ellipse affects the Q factor while the other parameters keep constant.

The following figures show that the frequency tends to drop by 8% when the value of the semi-major axis of ellipse increases from 500 μm to 625 μm as shown in Figure 24. Table 6 also shows that the normalized Q factor of this model reduces significantly by 27% (fused silica) and 28% (Vycor) with the higher value of semi-major axis of ellipse, respectively. Hence, it implies that the disc resonator with normal circle shape in 2D, is equipped with higher Q factor than the one with non-uniformity shape (ellipse).

	Semi-major axis [mm]	Normalized Q	Normalized displacement
Fused silica	500	1.0000	1.000000
	510	0.0083	0.000022
	520	0.0080	0.000016
	530	0.0079	0.000011
	540	0.0077	0.000010
	550	0.0075	0.000007
	560	0.0073	0.000007

Table 6: Normalized Q and displacement versus length of long axis of ellipse when $n=4$

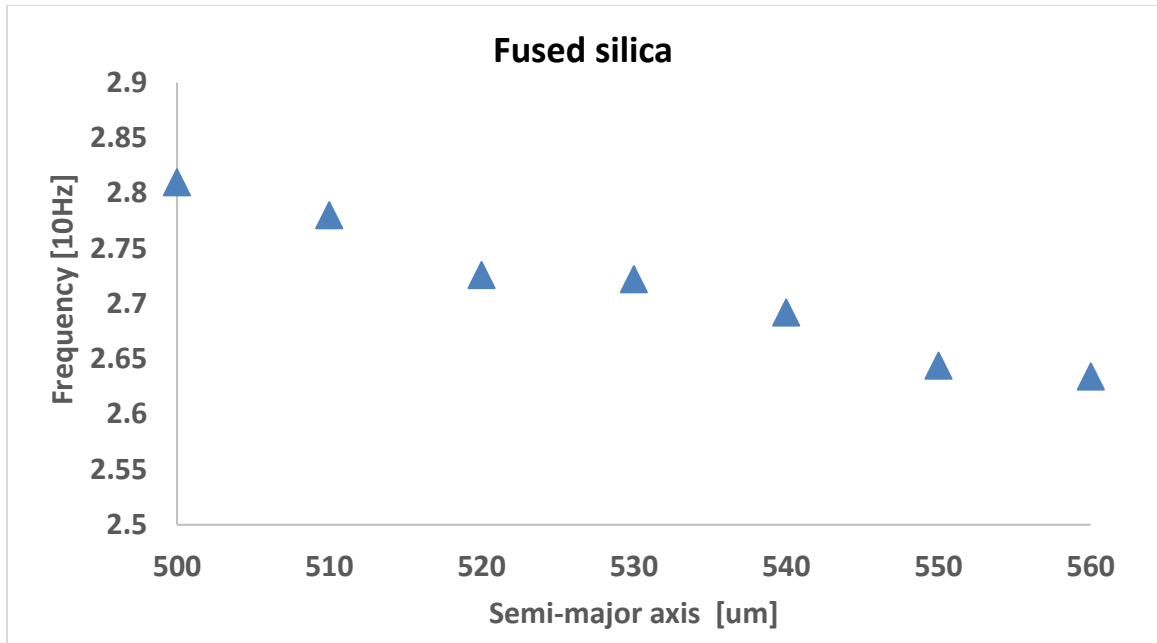


Figure 24: Frequency versus the value of semi-major axis respectively when $n=4$

3.4 Conclusion

This chapter analyzed the electro-mechanism coupling on the MEMS disc resonator gyroscope numerically, which is based on the geometric dimensions and material properties. Material properties were comprehensively analyzed in the above sections. The results obtained from the simulation indicate that a higher Young's modulus, lower density and lower Poisson's ratio of the resonator material can increase the frequency, Q factor and displacement of nodal point for the disc resonator gyroscopes. For example, reducing the density of the material of the model by 40% can increase both the frequency and Q factor by around 10%; decreasing the Poisson's ratio by 40% can slightly raise the Q by 5%. Geometric aspects (dimensions) also matter for the performance of disc resonators (based on fused silica and polysilicon). The results obtained show that the Q factor tends to increase with the rise of thickness of the disc, the decrease of gap length between disc and electrodes, and the decrease of radius of disc. For example, the resonator made of polysilicon had 97.5% of the Q factor and 94% frequency when the radius of the disc was increased by 5%. This chapter also discusses the investigation of the non-uniformity shape during simulation, such as ellipse shaped disc. The data obtained from the model implies that Q factor of this model reduces significantly by 27% (fused silica) and 28%

(Vycor) with the higher value of semi-major axis of ellipse, respectively. As a result, the above methods and elements can help optimize the DRG with ultra-high accuracy.

Chapter 4: Fabrication

4.1 Fabrication of hemispherical resonators

4.1.1 Introduction

In terms of fabrication for the HRG, the batch production for the three dimensional wineglass devices is challenging. That is because the HRG needs to be extremely symmetric and round in shape [35]. Previous axisymmetric ring gyroscopes have been investigated in 2D, such as the disc resonator gyroscope [36]. Recently, Senkal et al. demonstrated a MEMS fabrication process based on glassblowing for building symmetric 3-D wineglass and spherical shell structures in microscale [37]. They also used low internal loss materials, such as fused quartz and ultra-low expansion Titania silicate glass for the fabrication of 3-D wineglass shell structure. D. Senkal's approach successfully enabled the new MEMS device with extremely low surface roughness, low thermoelastic dissipation and relatively high symmetric structures [37].

4.1.2 Fabrication process

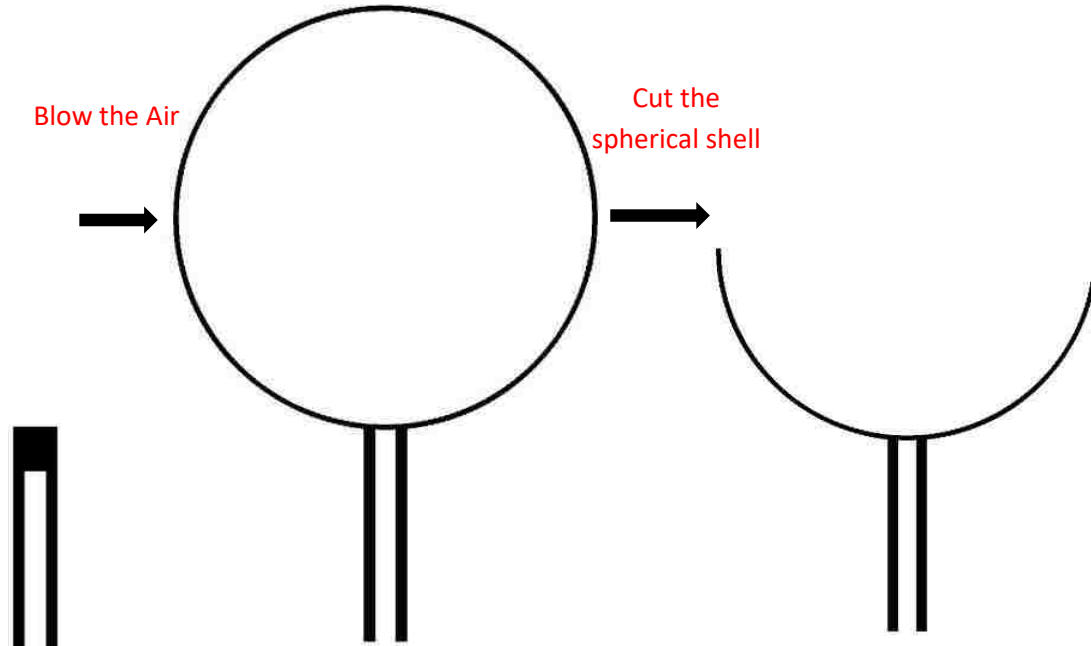


Figure 25: Basic process of glassblowing techniques for hemispherical resonator

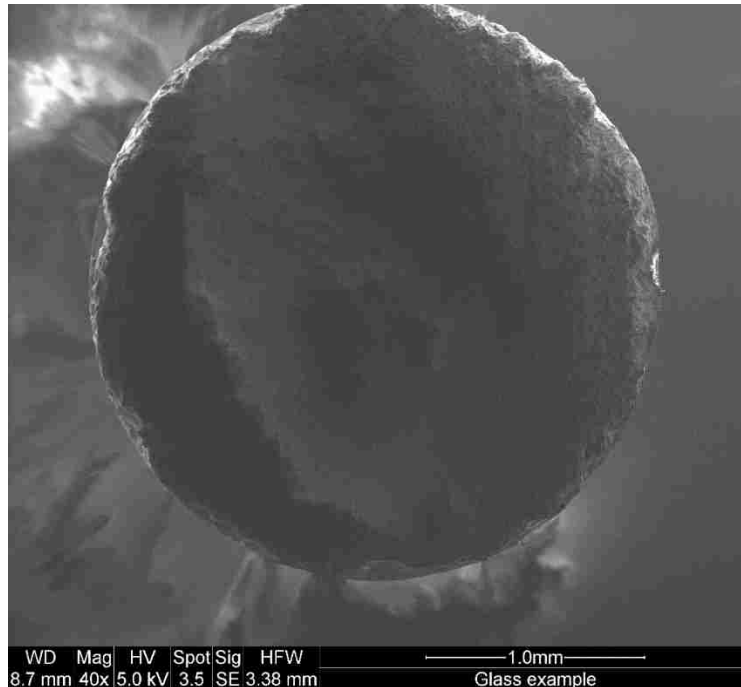


Figure 26: SEM image for fabricated hemispherical resonator

Glassblowing technique was utilized to fabricate a 3D MEMS hemispherical resonator. The fabrication process is similar to [37]. The glassblowing technique is applied for the fabrication of the resonator because it is a cost-effective process and optical for building a highly axisymmetric mode. Glassblowing is a glass-forming technique. It involves inflating molten glass into a bubble by a blowpipe. As shown in Figure 25, the steps of fabrication are listed below. At first, the wafer stack was heated up to the softening point of the glass layer. Then the glass layer became viscous and the air pressure inside was higher than the atmospheric pressure, which resulted in the pressure difference [37]. Due to the pressure difference and the surface tension between the outside and inside parts, plastic deformation kept going in the glass layer, until the pressure inside and outside reached equilibrium [37]. Therefore, a highly symmetric shell of fused silica was produced. The next step was cutting the spherical one into a wineglass shape structure. So a 1mm thickness and 5mm radius fused silica hemispherical wineglass resonator with a stem (5mm length and 1mm radius) was fabricated as shown in Figure 26.

The scanning electron microscope (SEM) can produce images of a sample by scanning it with a focused beam of electrons. It can be used to scan the sample surfaces and observe if there are flaws or defects on the samples. The clear screen shot from SEM is shown in Figure 25.

At the next step, Acetone is used in the wash process for cleaning purpose. However, Acetone may leave some residue, so IPA is used to displace water, allowing the sample surfaces to dry without spotting. The reason why I do not use methanol is that it is more flammable and toxic than IPA even though it works better. On top of that, a carbon deposit may be applied on the samples, which can help obtain a clearer image of my device from SEM.

4.2 Fabrication of disc resonator gyro [DRG]

4.2.1 Introduction

DRG was fabricated using conventional SOI (silicon on insulator) based fabrication process using microfabrication facility available at University of Toronto. Fabrication steps are shown in Figure 27. The first step is to clean the wafer followed by defining the etch mask using photolithography technology. Photolithography is a basic step used in the fabrication of MEMS structures. The principal of photolithography is based on the way that an amount of polymeric compound (photoresists) respond to exposure by UV light. The areas exposed to the UV light exhibits the selective solubility in a developing solution. There are two types of photoresist, including positive and negative photoresist. The positive resist is a type of photoresist. The portion of the positive photoresist can be exposed to light and become soluble to the photoresist developer, while the unexposed portion of the photoresist remains insoluble to the photoresist developer. Hence, the positive photoresist is what this fabrication of DRG requires. After defining the etch mask, the device layer is etched using dry etching to define the device and electrode gaps. Dry etching was done using deep reactive ion etching.

DRIE (deep reactive-ion etching) is a highly anisotropic etch process. It is used to create deep penetration, steep-sided holes and trenches in wafers with high-aspect-ratios. DRIE is a “dry” etching process and it is widely used in micro-fabrication. Compared with wet etching, dry etching has two main advantages: less undercutting which allows smaller lines to be patterned and higher anisotropy [38].

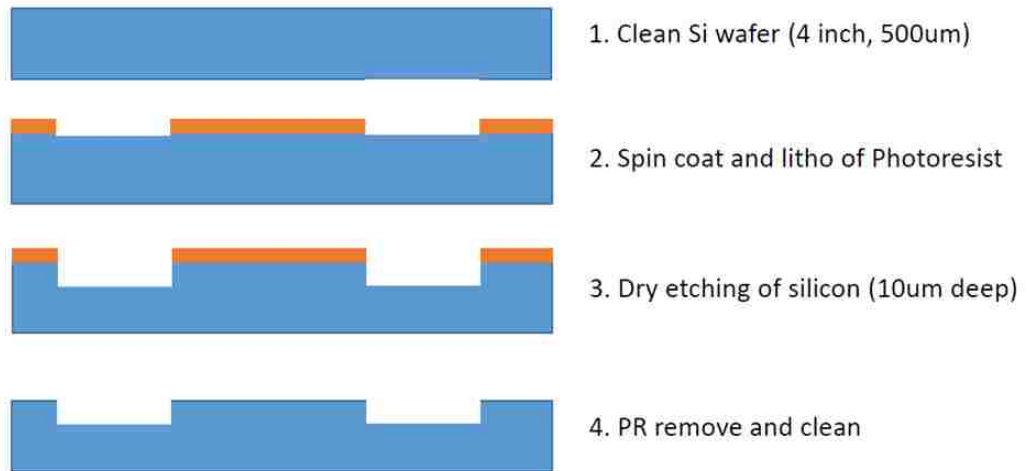


Figure 27: Schematic process of fabrication for DRG

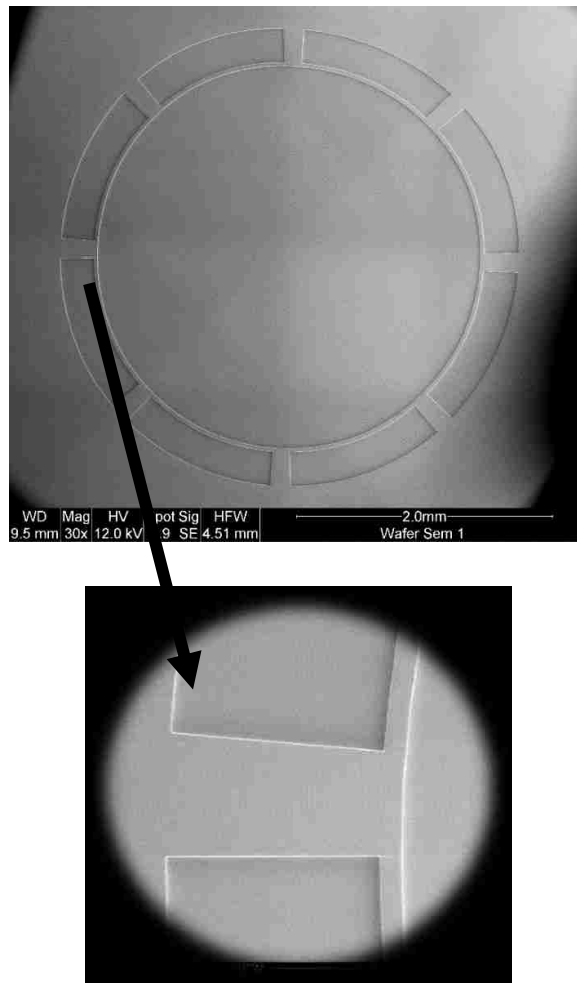


Figure 28: SEM for fabricated disc resonator device

4.2.2 Fabrication process

Detailed fabrication steps are shown in Figure 27.

4.2.2.1 Spin coating

Generally, spin coating is one of the most common techniques to apply the thin films to substrates. A significant number of industries and technology sectors are using this technique. Spin coating is able to produce the uniform films quickly and effectively and has a high consistency at both macros scale and micro scale. It also has some disadvantages, such as its fast drying times which can also lead to lower performance for some particular MEMS technologies. The key in this step is the spin speed and the spin coating duration. The range of spin speeds available is important, because it defines the range of thicknesses based on the given solution. Hence, 4000rpm was chosen as the spin speed. In order to dry the solvents (HMDS) fully, 30 seconds was set into a timer as the duration time.

4.2.2.2 Exposure

Exposure means producing an image on the wafer by a mask. Theoretically, the patterns on mask blocks some parts of the light and lets the others pass. This step is to transfer the patterns (image) from the mask to the wafer. The key in this step is the application of a mask contact aligner. By using vacuum chuck leveling system, the substrate is leveled quickly and gently in this machine for parallel photo mask alignment during contact exposure.

4.2.2.3 Develop

At this step, a container was used to mix 50mL developer and 150mL water. Afterwards, the wafer was submerged in the container and agitated.

4.2.2.4 Dry etching

Etching is the process of material being removed from the surface of wafer. Dry etching has some advantages, such as its capability of automation and reduced material consumption. Dry etching costs less to dispose of the products than wet etching. Since RIE combines both physical and chemical interactions, this process is relatively fast. The high-energy collision from the ionization is helpful for dissociating the etchant molecules into more reactive species. Hence, DRIE was applied on the wafer in this step. After this process, IPA was used to dissolve the photoresist on the wafer.

4.2.2.5 Inspection

This step was to observe how the patterns were etched and how deep the patterns were. Afterwards, SEM can be used to scan the device surfaces and observed the situation of edge defects on the patterns. The clear images were taken from SEM as shown in Figure 28.

Chapter 5: Conclusion

This thesis numerically analyzed the principle of energy loss mechanisms for two different types of resonators (hemispherical shell and disk) for different geometric and material properties. Minimizing the energy dissipation is critical to the development of resonators with high precision applications in gyroscopes and clocks. Also, in this thesis, MEMS based inertial resonators that has an ultra-high quality factor was developed. Investigation with loss-mechanism showed that the available mechanical materials offered ultra-low damping during the oscillation of DRG and HRG with a high Q factor.

In Chapter 2 of this thesis, a wineglass hemispherical resonator was created in the simulation. The thermo-elastic damping on the Q factor of the shell resonators was analyzed. This model is equipped with 12842 elements of mesh configuration and converges at 4.94×10^4 Hz. After the simulation, the results obtained show that the Q factor tends to increase with the rise of thickness of shell, the reducing of height, and the decrease of radius of the stem. For example, the higher thickness, which increases from 1 to 2 mm, can lead to 2.3 times of the normalized Q factor. The lower height of shell (from 6.5 to 3.5 mm) helped create a 1.3 times of Q factor. This thesis also proves that mass variation does not affect the simulation results when some of the parameters are changed. In terms of the non-uniformity shape of the resonator, it can enhance by the Q-factor. The results obtained show that non-uniformity, with a higher thickness of the bottom and a thinner edge, substantially increased the Q factor by 2.6 times of the normalized Q. The location of center of gravity of the resonator is also taken into consideration during the simulation. It was proven that the further the center of gravity is away from the bottom point of shell, the lower the Q factor, which means that the bonding point between the stem and the shell, located in the lowest point of the shell, can help obtain the higher Q factor. For instance, 2 mm offset from original bonding point can reduce 20% of the Q factor when the node of the mode shape is two. The effect of material properties can drastically change the Q factor. Among the different materials available, the cost effective ones such as Vycor can offer just half of the Q factor of fused quartz. An Irregular surface on the resonator is unavoidable during fabrication, and it creates a large amount of damping when the resonant structure vibrates. During the simulation, a regular curve surface was used to represent the edge defects. In this thesis, it was proven that about 35% of the Q factor was lost because of the

undesirable edge defects. As a result, in order to fabricate the MEMS resonator with high accuracy, minimizing thermos-elastic dissipation in the energy loss is critical.

Chapter 3 analyzed the electro-mechanism coupling on the MEMS disc resonator gyroscope numerically, which is based on the geometric dimensions and material properties. In this chapter, a disc shaped resonator was created with a stem and surrounded by four conformal electrodes. In terms of material properties, the results from simulation illustrate that the effect of material properties can drastically change the Q factor. The higher Young's modulus, lower density and lower Poisson's ratio of the resonator material can increase the frequency, Q factor and displacement of nodal point for the DRG. For the Young's modulus as an example, doubling the Young's modulus while keeping the other material properties fixed can increase the Q factor by about 1.5 times and the displacement of nodal point by about 9 times. In the geometric factor, the results obtained show that the Q factor tends to increase with the rise of thickness of the disc, the decrease of gap length between disc and electrodes, and the decrease of radius of disc. For example, the resonator made of polysilicon has 97.5% of the Q factor and 94% frequency when the radius of the disc increases by 5%. Half of the thickness of the disc can just offer 66% (fused silica) of the Q factor. Increasing the gap between disc and electrodes from 10 mm to 35 mm can help the normalized Q factor surge from 0.4 to 1. Meanwhile, the frequency of the disc becomes smaller with a higher radius. Furthermore, a non-uniformity disc resonator shaped like an ellipse can drastically decrease the Q-factor, so the regular disc resonator helps to obtain the higher effectiveness of DRG. During the simulation for DRG, I did not take the cases of misalignment and edge defect into consideration. However, according to the results and discussions in Chapter 2, I believe that the TED also has the same effect on the DRG (compared with the HRG). As a result, the above methods in this chapter can help to optimize the DRG with ultra-high accuracy.

Chapter 4 illustrated the fabrication process about a hemispherical wineglass resonator and disc resonator, respectively. During the fabrication of the device, I took advantages of the 3-D wineglass architecture, fabrication techniques with low surface roughness, and the materials with high isotropy and low TED. Glassblowing technique is optimal to fabricate the device because it is a cost-effective process and optimal to build a highly axisymmetric mode. After the device was done, SEM was used to scan the sample surfaces and observe if there were flaws or defects on the samples. If necessary, a coating can also be applied on the surface of the

resonator sample, which may help get a clearer image from SEM. For the fabrication of disc resonator, all the steps and details were listed when the disc resonator was fabricated. The fabrication steps included spin coating, exposure, dry etching and inspection. Among them, dry etching is the most vital step, because it helps to transfer the patterns from the mask to wafers, so this step needs the most time and carefulness. When the fabrication of the device was finished, SEM was also required to scan the surface of the device, and observe if the patterns were clear and complete.

All the results in the thesis can be applied to optimize the designing of MEMS based 3D resonators. MEMS devices require more reliability research in order to predict the desire performance under different environments and operation conditions. The future works in this field should consider the reduction of damping, as well as the integration of different sensors on a single chip for monitoring several physical parameters. Enhancing the Q-factor can further enable the development of high precision resonators and gyroscopes.

REFERENCES/BIBLIOGRAPHY

- [1] A.A. Trusov, "Overview of MEMS gyroscopes: history, principles of operations, types of measurements," *MicroSystems Laboratory, Mechanical and Aerospace Engineering, University of California, Irvine, CA, USA*, 2011.
- [2] H. Moeenfard, M.T. Ahmadian, and A. Farshidianfar, "Modeling squeezed film air damping in torsional micromirrors using extended Kantorovich method," *Meccanica*, vol. 48, Iss. 4, pp. 791–805, 2012
- [3] R. Lifshitz and M.L. Roukes, "Thermoelastic damping in micro- and nanomechanical systems," *Physical Review, B* 61, 5600, vol. 61, Iss. 8, 2000,
- [4] C. Li, M.H. Miller, "Investigation of Air Damping and Q in a MEMS Resonant Mass Sensor," *Proc. of the ASPE Annual Meeting*, 2008.
- [5] J. Wang, J.E. Butler, T. Feygelson, and C.T. Nguyen, "1.51-GHz nanocrystalline diamond micromechanical disk resonator with material-mismatched isolating support," *Micro Electro Mechanical Systems, 17th IEEE International Conference on. (MEMS)*, 2004.
- [6] J. Wang, Z. Ren, and C.T. Nguyen, "1.156-GHz Self-Aligned Vibrating Micromechanical Disk Resonator," *IEEE Ultrasonics, Ferroelectrics, and Frequency Control Society*, 2004
- [7] T.H. Lee and A. Hajimiri, "Oscillator phase noise: A tutorial," *IEEE J. Solid-State Circuits*, vol. 35, pp. 326–336, 2000.
- [8] N.C. Tsai, J.S. Liou, C.C. Lin, and T. Li, "Design of micro-electromagnetic drive on reciprocally rotating disc used for micro-gyroscopes," *Sens. Actuators A: Physical*, vol. 157, Iss.1, pp. 68–76, 2010.
- [9] D. Xia, C. Yu, and L. Kong, "The Development of Micromachined Gyroscope Structure and Circuitry Technology," *Sensors*, vol. 14, Iss1, pp. 1394-1473, 2014.
- [10] J. Liu, J. Jaekel, D. Ramdani, N. Khan, D.S. Ting, and M.J. Ahamed, "Effect of geometric and material properties on thermoelastic damping (TED) of 3D hemispherical inertial resonator," *Simulation*, Vol.1, pp.11, 2016.
- [11] J. Li, C. Guo, L. Mao, and J.Xu, "3D printed bandpass filters using compact high- Q hemispherical resonators with improved out-of-band rejection," *The Institution of Engineering and Technology*, Vol. 53, Iss. 6, pp. 413 – 415, 2016.
- [12] T. Zhang, Z. Lin, M. Song, B. Zhou, and R. Zhang, "Study on the thermoforming process of Hemispherical Resonator Gyros (HRGs)," *Inertial Sensors and Systems (INERTIAL)*, 2017 *IEEE International Symposium on Kauai, HI, USA*.

- [13] P. Pai, F.K Chowdhury, H. Pourzand, and M.T. Azar, "Fabrication and testing of hemispherical MEMS wineglass resonators," *Micro Electro Mechanical Systems (MEMS), IEEE 26th International Conference, Taiwan, China, 2013.*
- [14] M.M. Rahman, Y. Xie, C. Mastangelo, and H. Kim, "3-D hemispherical micro glass-shell resonator with integrated electrostatic excitation and capacitive detection transducers," *Micro Electro Mechanical Systems (MEMS), IEEE 27th International Conference, San Francisco, CA, USA, 2014.*
- [15] D. Senkal, M.J. Ahamed, A.A. Trusov, and A.M. Shkel "High temperature micro-glassblowing process demonstrated on fused quartz and ULE TSG," *Sensors and Actuators A*, vol. 201, pp. 525– 531, 2013.
- [16] D. Senkal, M.J. Ahamed, A.A. Trusov, and A.M. Shkel, "Electrostatic and mechanical characterization of 3-D micro-wineglass resonators," *Sensors and Actuators A*, vol. 215, pp. 150–154, 2014.
- [17] M. M. Rahman, Y. Xie, C. Mastrangelo, and H. Kim, "3-D hemispherical micro glass-shell resonator with integrated electrostatic excitation and capacitive detection transducers," *Micro Electro Mechanical Systems (MEMS), IEEE 27th International Conference on San Francisco, CA, USA, 2014.*
- [18] Hemispherical resonator gyroscope: <https://en.wikipedia.org/>. Last access on Nov.13th, 2017.
- [19] J. Wang, J. Ren, and C. T. Nguyen, "Self-aligned 1.14-GHz vibrating radial-mode disk resonators," *Transducers '03*, pp. 947-950, 2003.
- [20] J. R. Clark, T. Hsu, and C.T. Nguyenn, "High-Q VHF micromechanical contour-mode disk resonator," *Technical Digest, IEEE Int. Electron Devices Meeting, San Francisco, California*, pp. 493-496, 2000.
- [21] M. A. Abdelmoneum, M. U. Demirci, and C. T. Nguyen, "Stemless wine-glass-mode disk mech. resonators," *Micro Electro Mechanical System, MEMS-03 Kyoto. IEEE The Sixteenth Annual International Conference on Kyoto, Japan, 2003.*
- [22] A Silicon disc resonator gyroscope; <https://omnidimensionalcheesesandwich.wordpress.com/> Last access on Nov.13th, 2017.
- [23] K.Y. Yasumura, T.D. Stowe, E.M. Chow, T. Pfafman, T. W. Kenn, B.C. Stipe, and D. Rugar, "Quality factors in micron- and submicron-thick cantilevers," *IEEE Robotics and Automation Society*, vol. 9, p. 117-125, 2000.
- [24] R. Lifshitz, and M. L. Roukes, "Thermoelastic damping in micro- and nanomechanical systems" *Phys. Rev. Vol. 61, Iss. 8, pp.5600, 2000.*

- [25] A. Darvishian, B. Shiari, J. Y. Cho, T. Nagourney, and K. Najafi, "Investigation of Thermoelastic Loss Mechanism in Shell Resonators," *ASME 2014 International Mechanical Engineering Congress and Exposition, Micro- and Nano-Systems Engineering and Packaging, Montreal, 10*, pp. V010T13A062, 2013.
- [26] B. Shiari, and K. Najafi, "Surface effect influence on the quality factor of microresonators", *Transducers and Eurosensors XXVII, the 17th International Conference on Solid-State Sensors, Actuators and Microsystems*, 2013.
- [27] B.J. Hamrock, S.R. Schmid, and B.O. Jacobson, "Fundamentals of Fluid Film Lubrication," *Marcel Dekker, Inc.*, 2004
- [28] M. Weinberg, R. Candler, S. Chandorkar, J. Varsanik, T. Kenny, and A. Duwell, "Energy loss in MEMS resonators and the impact on inertial and RF devices," *Sensor IEEE, Denver, CO, USA.*, 2009.
- [29] C.J. Adkins, "Equilibrium Thermodynamics," *Cambridge University Press*, 1983.
- [30] W. Yourgrau, A.V.D. Merwe, and G. Raw, "Treatise on Irreversible and Statistical Thermodynamics: An Introduction to Nonclassical Thermodynamics," *Dover Publications, Inc.*, 2002.
- [31] C. Zener, "Internal Friction in Solids II: General Theory of Thermoelastic Internal Friction," *Physical Review*, vol. 53, pp. 230–235, 1938.
- [32] *Comsol Multiphysics Package*; <http://www.comsol.com>. Last access on Nov.13th, 2017.
- [33] M.J. Ahamed, D. Senkal, and A.M. Shkel, "Effect of Annealing on Mechanical Quality Factor of Fused Quartz Hemispherical Resonator," *International Symposium on Inertial Sensors and Systems, Laguna Beach (ISISS), CA*, pp. 1-4, 2014.
- [34] J. R. Clark, M. A. Abdelmoneum, and C. T. Nguyen, "High-Q UHF micromechanical radial-contour mode disk resonators," *Journal of Microelectromechanical Systems*, vol.14, issue. 6, 2005.
- [35] J. J. Bernstein, M. G. Bancu, J. M. Bauer, E. H. Cook, P. Kumar, E. Newton, T. Nyinjee, G. E. Perlin, J. A. Ricker, W. A. Teynor, M. S. Weinberg, "High Q diamond hemispherical resonators: fabrication and energy loss mechanisms", *J. Micromech. Microeng.*, vol. 25, pp. 1-12, 2015.
- [36] H. G. Howard, and A.D. Challoner, "Environmentally robust disc resonator gyroscope," *US patent # 8393212 B2*, 2013.
- [37] D. Senkal, M.J. Ahamed, A.A. Trusov, and A.M. Shkel, "Electrostatic and mechanical characterization of 3-D micro-wineglass resonators," *Sensors and Actuators A: Physical* vol. 215, pp.150-154, 2014.

[38] J. Bhardwaj, H. Ashraf, A. McQuarrie, "Dry silicon etching for MEMS," *The Symposium on Microstructures and Microfabricated Systems at the Annual Meeting of the Electrochemical Society, Montreal, Quebec, Canada, 1997.*

VITA AUCTORIS

NAME: Jiewen Liu (Nicky)

PLACE OF BIRTH: Windsor, ON

YEAR OF BIRTH: 1989

EDUCATION: South China University of Technology, B.Sc., China,
2012

University of Windsor, M.Eng, Windsor, ON, 2014

University of Windsor, M.Sc., Windsor, ON, 2016